CMI

www.nature.com/cmi

ARTICLE

# CIS controls the functional polarization of GM-CSF-derived macrophages

Shengbo Zhang[1,2,11], Jai Rautela[3,4,11], Naiara G. Bediaga[1,2,11], Tatiana B. Kolesnik[1,11], Yue You[1,2], Junli Nie[1,2], Laura F. Dagley[1,2], Justin Bedo[1,5], Hanqing Wang[6], Li Sun[7], Robyn Sutherland[1,2], Elliot Surgenor[1], Nadia Iannarella[1], Rhys Allan[1,2], Fernando Souza-Fonseca-Guimaraes[8], Yi Xie[1,9], Qike Wang[1,2], Yuxia Zhang[6], Yuekang Xu[7], Stephen L. Nutt[1,2], Andrew M. Lew[1,2], Nicholas D. Huntington[3,4,12], Sandra E. Nicholson[1,2,12], Michaël Chopin[1,2,3,12]✉ and Yifan Zhan[1,2,10,12]✉



The cytokine granulocyte-macrophage-colony stimulating factor (GM-CSF) possesses the capacity to differentiate monocytes into macrophages (MØs) with opposing functions, namely, proinflammatory M1-like MØs and immunosuppressive M2-like MØs. Despite the importance of these opposing biological outcomes, the intrinsic mechanism that regulates the functional polarization of MØs under GM-CSF signaling remains elusive. Here, we showed that GM-CSF-induced MØ polarization resulted in the expression of cytokine-inducible SH2-containing protein (CIS) and that CIS deficiency skewed the differentiation of monocytes toward immunosuppressive M2-like MØs. CIS deficiency resulted in hyperactivation of the JAK-STAT5 signaling pathway, consequently promoting downregulation of the transcription factor Interferon Regulatory Factor 8 (IRF8). Loss- and gain-of-function approaches highlighted IRF8 as a critical regulator of the M1-like polarization program. In vivo, CIS deficiency induced the differentiation of M2-like macrophages, which promoted strong Th2 immune responses characterized by the development of severe experimental asthma. Collectively, our results reveal a CIS-modulated mechanism that clarifies the opposing actions of GM-CSF in MØ differentiation and uncovers the role of GM-CSF in controlling allergic inflammation.

**Keywords:** CIS; GM-CSF; Macrophage; M2; M1

*Cellular & Molecular Immunology* (2023) 20:65–79; https://doi.org/10.1038/s41423-022-00957-z

## INTRODUCTION

Macrophages (MØs) play crucial roles in immune defense against invading pathogens and have important functions in regulating and maintaining tissue homeostasis [1]. It has long been appreciated that MØs show functional plasticity/polarization and dynamically respond to different physiological situations. External cues, including cytokines and Toll-like receptor (TLR) agonists, can direct MØ functional polarization [2]. Historically, interferon (IFN)-γ and interleukin (IL)-4 have been used to induce polarization of classically activated M1 MØs with strong proinflammatory functions and alternatively activated M2 MØs with anti-inflammatory functions, respectively [2].

Differing from the aforementioned modes of MØ polarization, MØs generated from bone marrow (BM) progenitors or monocytes in the presence of granulocyte-macrophage-colony stimulating factor (GM-CSF) or macrophage-colony stimulating factor (M-CSF), respectively, can display both M1- and M2-like characteristics [3]. GM-CSF-differentiated MØs are thought to be M1-like, producing proinflammatory cytokines upon stimulation with TLR ligands [3–5]. Corroborating evidence from an autoimmune disease context supports a proinflammatory role for GM-CSF in vivo (reviewed in [6, 7]). Consistent with its proinflammatory properties, GM-CSF has long been used in the vaccination setting as a strong immune adjuvant to promote antitumor immunity [8].

Paradoxically, GM-CSF has also been associated with the development of suppressive M2-like MØs in various tumor settings [9–11] and after renal ischemia [12]. GM-CSF also has a critical role in the induction of allergic inflammation [13, 14], and consequently, its neutralization was found to dampen inflammation in certain allergic settings [13], although it is not clear that M2-like MØs are directly responsible for the induction of allergic inflammation. Nevertheless, M2-like MØs are known to support Th2 immunity [15]. A protective role for GM-CSF in murine models of dextran sulfate sodium (DSS)-induced colitis was also associated with GM-CSF-induced myeloid cells [16]. Together, these studies

[1]Walter and Eliza Hall Institute of Medical Research, Parkville, VIC, Australia. [2]Department of Medical Biology, University of Melbourne, Parkville, VIC, Australia. [3]Department of Biochemistry and Molecular Biology, Biomedicine Discovery Institute, Monash University, Clayton, VIC, Australia. [4]oNKo-Innate Pty Ltd, Moonee Ponds, VIC, Australia. [5]Department of Computing and Information Systems, University of Melbourne, Parkville, VIC, Australia. [6]Department of Respiratory Medicine, Guangzhou Institute of Pediatrics, Guangzhou Women and Children's Medical Centre, State Key Laboratory of Respiratory Diseases, Guangzhou Medical University, Guangzhou, Guangdong, China. [7]College of Biological Science, Anhui Normal University, Hefei, China. [8]University of Queensland Diamantina Institute, University of Queensland, Translational Research Institute, Brisbane, QLD, Australia. [9]Program in Cardiovascular and Metabolic Disorders, Duke-NUS Medical School, Duke, Singapore. [10]Drug Discovery, Shanghai Huaota Biopharm, Shanghai, China. [11]These authors contributed equally: Shengbo Zhang, Jai Rautela, Naiara G Bediaga, Tatiana B Kolesnik. [12]These authors jointly supervised this work: Nicholas D Huntington, Sandra E Nicholson, Michaël Chopin, Yifan Zhan. ✉email: Michael.chopin@monash.edu; yifan.zhan@huabobio.com

Received: 18 June 2022 Revised: 24 October 2022 Accepted: 7 November 2022
Published online: 5 December 2022

point to divergent functional outcomes driven by GM-CSF signaling in MØs, yet the molecular mechanism governing the functional dichotomy of the effects of GM-CSF on MØs is largely unknown.

The strength and duration of GM-CSF signaling are tightly regulated by the induction of suppressors of cytokine signaling (SOCS) proteins, which act in a negative feedback loop to limit cytokine responses [17, 18]. Among the SOCS family members, cytokine-inducible SH2 protein (CIS) is a known target of STAT5 activation [19–21] and is induced by GM-CSF in MØs [19, 22]. CIS-deficient mice housed in a specific pathogen-free environment showed no overt defects in myelopoiesis, suggestive of low GM-CSF or CIS expression in an unchallenged situation [23, 24]. In line with this, the impact of CIS deficiency in natural killer (NK) cells or T cells became apparent only following stimulation with exogenous IL-15 or T cell receptor (TCR) engagement, respectively [25–27].

Here, we explored the role of CIS in regulating MØ functional polarization following GM-CSF stimulation. We found that CIS deficiency resulted in the development of MØs with strong immunosuppressive functions, limited production of IL-12 and an M2-like MØ gene signature that ultimately induced a Th2-biased immune response in vivo. The functional skewing was largely the result of hyperactivation of the JAK-STAT5 signaling pathway, which led to suboptimal IRF8 induction and thus crippled the M1-like polarization program. Thus, our study highlights a critical role for CIS in fine-tuning GM-CSF signaling and promoting M1-like features in macrophages.

## RESULTS

### CIS deficiency leads to the generation of MØs that strongly inhibit T-cell responses

In line with previous studies [23, 26], we did not observe any conspicuous changes in the frequencies of myeloid cell types or BM hematopoietic progenitors in *Cish*$^{-/-}$ mice (Figs. S1 and S2). To investigate the role of CIS in MØ differentiation, we cultured BM progenitors from WT and *Cish*$^{-/-}$ mice [26] for 7 days with GM-CSF to generate MØs (GM-MØs; CD11c$^{+}$MHCII$^{int}$ CD11b$^{hi}$CD115$^{hi}$CD86$^{lo}$Flt3$^{lo}$) and dendritic cells (DCs) (GM-DCs; CD11c$^{+}$MHCII$^{hi}$CD11b$^{int}$CD115$^{-}$CD86$^{hi}$Flt3$^{hi}$) [28] (Fig. 1A). GM-MØs dominated in both genotypes (80–90% of total CD11c$^{+}$ cells), with a small but significant reduction in the proportion of GM-DCs in *Cish*$^{-/-}$ BM cell cultures (Fig. 1A). Flow cytometry and fluorescence microscopy experiments revealed that *Cish*$^{-/-}$ GM-MØs were larger in size than WT GM-MØs (Fig. 1B). We also found that *Cish*$^{-/-}$ GM-MØs had lower cell-surface expression of CD115 (Macrophage-Colony Stimulating Factor receptor; M-CSFR) than WT GM-MØs, while GM-MØs of both genotypes expressed similar levels of the GM-CSF receptor (GM-CSFR) α and β subunits (Fig. 1C). Downregulation of CD115 by GM-CSF was dose dependent and cell intrinsic since *Cish*$^{-/-}$ GM-MØs derived from a coculture containing WT cells also had lower CD115 expression (Fig. S3A, B). Similarly, the expression of other myeloid markers, such as CD209, CCR2, F4/80 and CD14, was reduced in *Cish*$^{-/-}$ GM-MØs compared to their WT counterparts (Fig. S3B, C). In contrast, CIS deficiency in GM-DCs had a limited impact on the expression of multiple cell-surface markers (Fig. S3D).

Next, we sought to compare the functions of GM-MØs generated from WT or *Cish*$^{-/-}$ mice. First, we evaluated GM-MØs for their ability to stimulate antigen-specific T-cell proliferation. To this end, GM-MØs were pulsed with ovalbumin (OVA) and subsequently cocultured with dye-labeled MHCI- and MHCII-restricted OVA-specific CD8$^{+}$ or CD4$^{+}$ T cells (OT-I and OT-II cells, respectively). T-cell proliferation was significantly weaker when T cells were cocultured with OVA-pulsed *Cish*$^{-/-}$ GM-MØs than when T cells were cocultured with OVA-pulsed WT GM-MØs (Fig. 1D, Fig. S3E). A similar observation was made for GM-DCs (Fig. S3E), suggesting that CIS expression in MØs is required to promote T-cell expansion. In line with the above findings, adoptive transfer of OVA-pulsed GM-MØs into C57BL/6 mice that had previously received GFP$^{+}$ OT-I cells revealed that antigen-driven T-cell expansion and IFN-γ production were weaker in mice vaccinated with OVA-pulsed *Cish*$^{-/-}$ GM-MØs than those vaccinated with WT GM-MØs (Fig. 1E, F). The difference in the T-cell responses induced by WT and *Cish*$^{-/-}$ GM-MØs was not due to antigen uptake or processing, since GM-MØs of both genotypes had a similar uptake and processing capacity (Fig. 1G). Moreover, when we bypassed antigen uptake/presentation by stimulating purified CD8$^{+}$ T cells with anti-CD3/anti-CD28 antibodies, *Cish*$^{-/-}$ GM-MØs (at MØ:T-cell ratios of 1:1 and 1:2) were more potent in suppressing T-cell proliferation and IFN-γ production than were WT GM-MØs (Fig. 1H). Thus, we conclude that CIS deficiency leads to the generation of MØs that inhibit T-cell expansion.

### CIS deficiency leads to the generation of mouse and human MØs with reduced IL-12 production

We next investigated the mechanism underlying the lack of IFN-γ production by CD8$^{+}$ T cells cocultured with *Cish*$^{-/-}$ GM-MØs (Fig. 1F, H). As IL-12 is a key cytokine promoting IFN-γ production [29], we measured IL-12 production by MØs upon TLR agonism. Compared to WT GM-MØs, *Cish*$^{-/-}$ GM-MØs produced substantially less IL-12 when stimulated with CpG or LPS (Fig. 2A, Fig. S4A). WT and *Cish*$^{-/-}$ BM coculture experiments confirmed that the reduced IL-12 production of *Cish*$^{-/-}$ GM-MØs was cell intrinsic (Fig. 2B). IL-12 production was also reduced in *Cish*$^{-/-}$ GM-MØs following stimulation with PolyI:C or an agonistic anti-CD40 antibody (Fig. S4B). The requirement for CIS was relatively selective for IL-12, as the expression of other cytokines (e.g., IL-6, IL-10 and TNF-α) was similar between WT GM-MØs and *Cish*$^{-/-}$ GM-MØs (Fig. S4C). The defective IL-12 production by *Cish*$^{-/-}$ GM-MØs was observed across a range of GM-CSF concentrations (Fig. S4D). In line with earlier reports [28, 30], GM-DCs produced less IL-12 than GM-MØs, and IL-12 production was CIS independent (Fig. S4E). These results suggest that CIS plays a critical role in promoting IL-12 production by GM-MØs.

The limited number of splenic MØs (identified as CD11c$^{+}$CD11b$^{+}$CD209$^{+}$FceR1$^{+}$ cells) in mice, probably due to the low abundance of GM-CSF in unchallenged mice [31, 32], precluded us from corroborating the above findings in vivo. To circumvent this issue, we challenged WT or *Cish*$^{-/-}$ mice for 9 days with a B16 melanoma cell line producing GM-CSF (B16-GM) [8]. When splenocytes isolated from challenged WT or *Cish*$^{-/-}$ mice were stimulated with CpG or LPS, we found that IL-12 production was substantially reduced in the absence of CIS (Fig. 2C). To evaluate the contribution of MØs to IL-12 production, we generated mixed bone marrow chimeric mice by reconstituting lethally irradiated recipient mice (C57BL/6-Ly5.1) with mixed WT (Ly5.1) and *Cish*$^{-/-}$ (Ly5.2) BM cells. Following reconstitution, the mice were engrafted with B16-GM cells for 9 days. MØs of both WT origin and *Cish*$^{-/-}$ origin were then isolated and stimulated with CpG for 20 h. Similar to in vitro-generated GM-MØs, splenic *Cish*$^{-/-}$ MØs isolated from B16-GM cell-bearing mice produced significantly less IL-12 than WT MØs (Fig. 2D).

Finally, we investigated whether CIS deficiency also impacted the capacity of human MØs to produce IL-12. To this end, CD34$^{+}$ cells derived from human cord blood were electroporated with Cas9 assembled in a ribonucleoprotein particle (RNP) with *CISH* guide (g) RNA. The indel frequency for donor CD34$^{+}$ cells transfected with CIS guide-RNPs was 83% (based on next-generation sequencing). Transfected CD34$^{+}$ cells were cultured with human GM-CSF (5 ng/mL) for 7–10 days. *CISH* gRNA- and mock-transfected cells differentiated into CD14$^{+}$CD16$^{+}$ cells. Notably, the percentage of CD14$^{+}$CD16$^{+}$ cells was higher in cultures with *CISH* gRNA than those that underwent mock transfection (Fig. 2E). When cells were

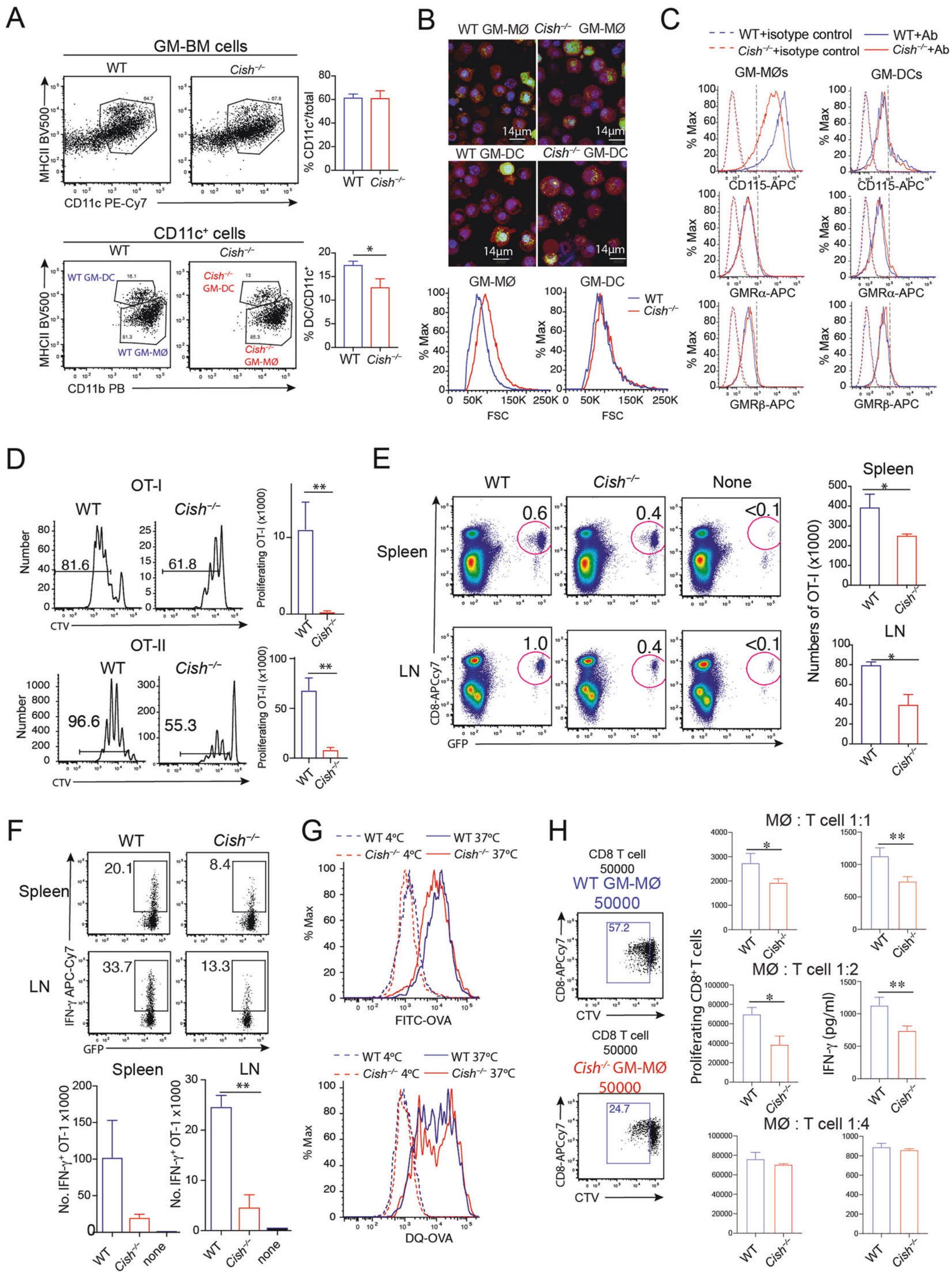

**Fig. 1** Cish−/− GM-MØs have a reduced capacity to induce T-cell responses. **A** WT and *Cish*$^{-/-}$ GM-MØ BM cells were cultured with 10 ng/mL GM-CSF for 7 days. Harvested cells were analyzed to identify GM-MØs and GM-DCs. **B** Sorted GM-MØs and GM-DCs were stained with CellTracker violet (red), LysoTracker green (green) and SIR-DNA (blue). Histograms showing cell size measured from the forward scatter data for WT and *Cish*$^{-/-}$ GM-MØs and GM-DCs. **C** Histograms showing the expression of M-CSF (CD115) and GM-CSF receptors (GMRα and GMRβ) on WT and *Cish*$^{-/-}$ GM-MØs and GM-DCs. **D** CTV-labeled OT-I or OT-II T cells were cultured with WT or *Cish*$^{-/-}$ GM-MØs in the presence of ovalbumin (OVA). Bar graphs represent the mean number ± S.D. of proliferating OT-I T cells at 48 h (top) and OT-II T cells at 60 h (bottom). Data are representative of three independent experiments. **E** B6 mice that had been previously injected with GFP-OT-I cells were intravenously infused with OVA-pulsed WT ($n = 3$) or *Cish*$^{-/-}$ GM-MØs ($n = 3$). *$P < 0.05$, Student's t test. Antigen-induced T-cell expansion was evaluated 5 days after MØ transfer. **F** IFN-γ production by GFP-OT-I cells was evaluated after 4 h of stimulation with PMA/ionomycin. **$P < 0.01$, Student's *t* test. Data are representative of two independent experiments. **G** Antigen uptake and processing of soluble OVA by WT and *Cish*$^{-/-}$ GM-MØs. For antigen uptake, cells were incubated with FITC-OVA at 37 °C or on ice for 30 min. For antigen processing, cells were incubated with DQ-OVA at 37 °C for 30 min. Then, the samples were either incubated at 37 °C for an additional 90 min or kept on ice. **H** Purified CD8$^{+}$ T cells from B6 mice were stimulated with anti-CD3/anti-CD28 antibodies with the indicated number of WT or *Cish*$^{-/-}$ GM-MØs for 3 days. Cell proliferation and cytokine production were then determined. *$P < 0.05$, **$P < 0.01$; Student's *t* test

stimulated with CpG or LPS, the production of IL-12 by cells targeted with *CISH* gRNA was substantially reduced compared to that of mock-transfected cells (Fig. 2E). Taken together, these data point to a critical role for CIS in controlling the production of IL-12 in both mouse and human MØs.

**CIS deficiency imprints MØs with M2-like characteristics**

We showed above that *Cish*$^{-/-}$ MØs strongly inhibited T-cell responses and had reduced IL-12 production compared to WT MØs. To gain insights into the molecular mechanisms underlying these functional changes, we performed RNA sequencing (RNA-seq) of sorted GM-MØs and GM-DCs from WT and *Cish*$^{-/-}$ mice ($n = 4$). Principal component analysis (PCA) revealed that CIS and cell lineage identity accounted for the major differences between the WT and *Cish*$^{-/-}$ samples. The impact of CIS deficiency was more prominent in GM-MØs than in GM-DCs, as evidenced by the increased separation of the MØ groups in the PCA plot (Fig. 3A) and the higher number of differentially expressed genes (DEGs) between the *Cish*$^{-/-}$ and WT samples (1029 and 713 DEGs for GM-MØs and GM-DCs, respectively) (Supplementary Table 1). As MØs are the dominant cell type generated under GM-CSF culture conditions and are more profoundly impacted by CIS deficiency, we chose MØs for further detailed analysis. Gene ontology analysis highlighted many differences between WT and *Cish*$^{-/-}$ GM-MØs that correlated with their differences in function, cell cycling and metabolism (Fig. S5A).

GM-CSF is thought to bias MØ polarization toward the proinflammatory M1-like state [3, 4], and we therefore expected that CIS deficiency would strengthen GM-CSF signaling and further increase M1 MØ polarization. Instead, analysis of the RNA-seq data indicated that the genes upregulated in *Cish*$^{-/-}$ GM-MØs were positively correlated with gene signatures derived from IL-4-induced M2 MØs (GSE25088) [33] and GSE32164 [34] (Fig. 3B). Next, we analyzed genes known to be associated with MØ functional polarization among the DEGs in *Cish*$^{-/-}$ GM-MØs [35, 36] (Supplementary Table 2). Over 64% (35/56) of the known M2 MØ-associated DEGs (Supplementary Table 2) were upregulated in *Cish*$^{-/-}$ GM-MØs (Fig. 3C), including prototypic genes such as *Chil3 (Ym1), Chil4, Retnla (Fizz1) and Tgm2*, while over 85% (26/30) (Supplementary Table 2) of the known M1 MØ-associated DEGs were downregulated in *Cish*$^{-/-}$ GM-MØs, thus suggesting that CIS deficiency skews GM-CSF-induced MØs toward an M2-like phenotype.

We also compared the DEGs to the gene signature of M-CSF-derived M2-like macrophages [37]. We found that the genes downregulated in *Cish*$^{-/-}$ GM-MØs were more strongly positively correlated with the gene signatures decreased in M-CSF-derived M2-like MØs compared with those in GM-CSF-derived M1-like macrophages (Fig. S5C). On the other hand, the genes upregulated in *Cish*$^{-/-}$ GM-MØs did not correlate with those upregulated in M-CSF-derived MØs (Fig. S5C) but instead positively correlated with gene signatures derived from IL-4-induced M2 MØs (Fig. 3B). Thus, *Cish*$^{-/-}$ GM-MØs resemble M-CSF-derived MØs in certain aspects but differ from them in other key parameters.

To support our transcriptomic analysis, we also performed label-free quantitative proteomic analysis of GM-MØs derived from WT and *Cish*$^{-/-}$ mice ($n = 4$) (Supplementary Table 3). In accordance with the transcriptional data, we found that several typical M2 MØ-associated proteins were upregulated in *Cish*$^{-/-}$ GM-MØs, including Arg1, Chil3, Tgm2 and Dab2 (Fig. 3D). In contrast, the proteins that were downregulated in *Cish*$^{-/-}$ GM-MØs included M1 MØ-associated proteins, such as CD74, Ass1 and Cybb (Fig. 3D). Overall, both the RNA-seq and proteomic analyses revealed that loss of CIS resulted in the development of GM-MØs sharing some features characteristic of M2-like MØs.

Next, we selected two commonly used M2 markers, Arg1 and Ym1, for further validation by western blotting. *Cish*$^{-/-}$ GM-MØs sorted from BM cultures derived from 3 individual mice all expressed higher levels of Arg1 and Ym1 than WT GM-MØs (Fig. 3E), thus corroborating the above results. To convert *Cish*$^{-/-}$ GM-MØs into M1-like MØs, we stimulated WT and *Cish*$^{-/-}$ GM-MØs with IFN-γ and LPS, potent M1 MØ-inducing cytokines. While IFN-γ and LPS treatment reduced the expression of Arg1 and Ym1 in both WT GM-MØs and *Cish*$^{-/-}$ GM-MØs, the latter retained substantially higher levels of these M2 MØ markers (Fig. S5B).

IL-4 is a prototypical cytokine that drives the differentiation of M2 MØs [36]. To investigate whether the M2-like phenotype of *Cish*$^{-/-}$ GM-MØs was influenced by endogenous IL-4, a neutralizing anti-IL-4 antibody was added to GM-CSF BM cell cultures on Day 5. *Cish*$^{-/-}$ GM-MØs maintained higher expression of Ym1 and Arg1 (Fig. 3F). Furthermore, addition of exogenous IL-4 in the late stage of cell differentiation increased the expression of Arg1 and Ym1 in GM-MØs, but these increases were comparable between the WT and *Cish*$^{-/-}$ genotypes (Fig. 3G). This observation suggests that the induction of the M2-like phenotype in *Cish*$^{-/-}$ GM-MØs is unlikely to be directly due to IL-4.

Finally, we examined the functional consequence of the high level of Arg1 in *Cish*$^{-/-}$ GM-MØs. Arginine availability is key to an optimal T-cell immune response [38]. As the Arginase 1 inhibitor L-norvaline enhances T-cell proliferation in the presence of antigen-presenting cells [39], we investigated whether inhibition of Arg-1 activity in *Cish*$^{-/-}$ GM-MØs could relieve the suppressive activity of *Cish*$^{-/-}$ GM-MØs (Fig. 1D–H). The addition of L-norvaline greatly enhanced the proliferation of OT-I T cells stimulated in the presence of *Cish*$^{-/-}$ GM-MØs but not that of those stimulated in the presence of WT GM-MØs (Fig. 3H). Thus, we contend that M2-phenotype molecular imprinting in the absence of CIS indeed leads to a gain of suppressive function, which can be partially relieved by inhibiting Arginase 1.

**Enhanced STAT5 activation in the absence of CIS contributes to the development of M2-like MØs**

Next, we investigated the signaling events leading to the development of M2-like features in the absence of CIS. Isolated GM-MØs that were rested and then restimulated with GM-CSF induced the mRNA and protein expression of CIS and STAT5 activation (measured as STAT5 tyrosine phosphorylation) in GM-MØs (Fig. 4A and B). Furthermore, CIS deficiency in GM-MØs led to enhanced and prolonged STAT5 activation after GM-CSF restimulation (Fig. 4C) but no differences in activation of the PI3K/Akt or ERK1/2 MAPK pathway (Fig. 4D).

To investigate whether enhanced JAK/STAT5 signaling is responsible for some of the functional changes observed in *Cish*$^{-/-}$ GM-MØs, we tuned down GM-CSF signaling using the JAK inhibitor ruxolitinib (RUXO, 0.2 μM). Hyperactivation of STAT5, but not Akt1 or ERK1/2, upon GM-CSF stimulation was also observed on Day 5 in BM-derived *Cish*$^{-/-}$ GM-MØs (Fig. 4E). The addition of RUXO to the medium substantially reduced the phosphorylation of STAT5 in both WT GM-MØs and *Cish*$^{-/-}$ GM-MØs (Fig. 4E). As expected, RUXO-treated GM-MØs also showed reduced phosphorylation of Akt1 and ERK1/2, whose activation depends on JAK kinase activation (Fig. 4E). Thus, these observations suggested that the impaired IL-12 production observed in *Cish*$^{-/-}$ GM-MØs (Fig. 2B and C) was independent of the activation statuses of Akt1 and ERK1/2. Importantly, the RUXO-mediated downmodulation of pSTAT5 restored the capacity of *Cish*$^{-/-}$ GM-MØs to produce IL-12 following CpG stimulation, and IL-12 production by WT GM-MØs was further enhanced by RUXO (Fig. 4F and G). This suggests that decreasing JAK/STAT5 signaling output in GM-MØs, which is normally mediated by CIS, is critical for optimal IL-12 production. The higher expression of Arg1 and Ym1 observed in *Cish*$^{-/-}$ GM-MØs was greatly reduced following RUXO addition to the cell culture (Fig. 4H). Taken together, these data suggest that CIS deficiency in GM-MØs results in increased activity of the JAK/STAT5 signaling pathway leading to the development of M2-like MØ features and reduced IL-12 production.

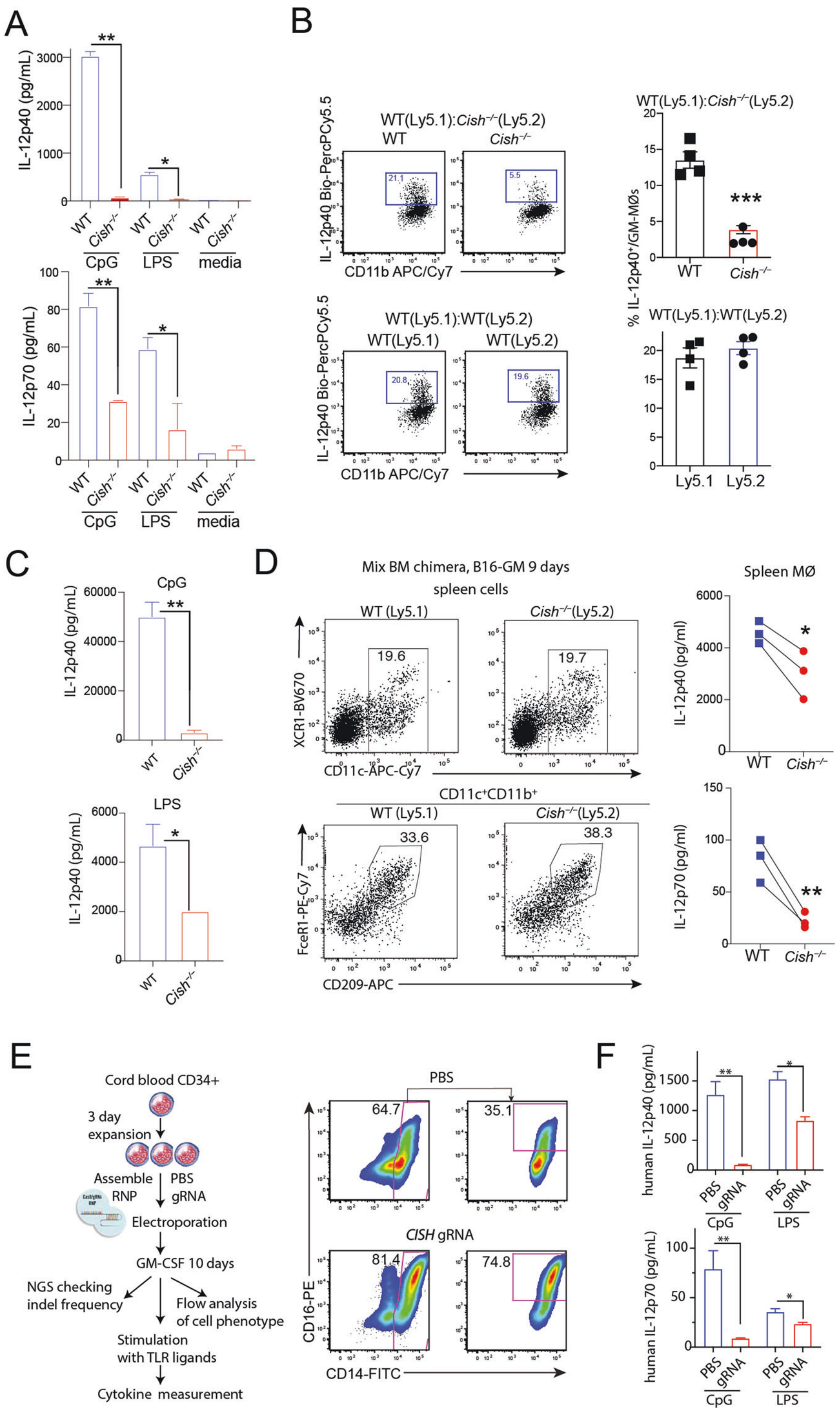


**Fig. 2** Cish−/− MØs produce a relatively low amount of IL-12. **A** IL-12 production by WT and *Cish*$^{-/-}$ GM-MØs stimulated with CpG or LPS for 20 h. *$P < 0.05$, **$P < 0.01$; multiple-group ANOVA. **B** Production of IL-12 by WT (Ly5.1) and *Cish*$^{-/-}$ (Ly5.2) GM-MØs derived from cocultures with BM cells isolated from individual mice. The harvested cells were stimulated with CpG for 4 h. ***$P < 0.001$, Student's *t* test. **C** IL-12 production by spleen cells isolated from WT or *Cish*$^{-/-}$ mice. Mice were engrafted with B16-GM cells for 9 days. Spleen cells were stimulated with CpG or LPS for 20 h. Bar graphs show the mean ± S.D. of the IL-12 concentration in culture supernatants. *$P < 0.05$, **$P < 0.01$; Student's *t* test. **D** IL-12 production by splenic MØs isolated from WT or *Cish*$^{-/-}$ mice. Mixed bone marrow chimeric mice reconstituted with both WT (Ly5.1) and *Cish*$^{-/-}$ (Ly5.2) BM cells were engrafted with B16-GM cells for 9 days. Sorted MØs were stimulated with CpG for 20 h. Line graphs show IL-12 production by paired WT and *Cish*$^{-/-}$ splenic MØs from the same host. *$P < 0.05$, **$P < 0.01$; Student's *t* test. **E**, **F** IL-12 production by human GM-MØs with *CISH* deletion. CD34$^{+}$ cells isolated from human cord blood were transfected with Cas9 assemble RNP and *CISH* guide RNA. The transfected CD34$^{+}$ cells were cultured with human GM-CSF (5 ng/ml) for 7 days. The cells were stimulated with CpG or LPS. **E** FACS plots show the resulting human GM-MØ population. **F** Bar graphs show IL-12 production by human GM-MØs. *$P < 0.05$, **$P < 0.01$; multiple-group ANOVA. Data are representative of three independent experiments

**Downregulation of IRF8 by enhanced STAT5 activation contributes to the development of M2-like MØs**

To define the molecular consequences of the sustained JAK/STAT5 activation observed in *Cish*$^{-/-}$ GM-MØs, we further analyzed our transcriptomic dataset. We focused our analysis on transcription factors known to regulate M1/M2 cell fate decisions, particularly the interferon responsive factor (IRF) family members known to be critical for MØ polarization [40]. Quantitation of the mRNA levels for the 9 members of this family revealed that only *Irf8* mRNA transcript levels were substantially reduced in *Cish*$^{-/-}$ GM-MØs compared to WT GM-MØs (Fig. 5A). To substantiate these findings, we crossed *Cish*$^{-/-}$ mice with *Irf8*$^{Gfp}$ reporter mice [41], allowing us to measure IRF8 expression at the single-cell level. GM-CSF reduced the expression of IRF8 in GM-MØs in a dose-dependent manner (Fig. 5B). Comparison of GM-MØs derived from *Irf8*$^{Gfp}$/WT and *Irf8*$^{Gfp}$/*Cish*$^{-/-}$ mice confirmed the reduced expression of IRF8 in GM-MØs lacking CIS (Fig. 5B). Consistent with this observation, the expression of IRF8 was substantially reduced in MØs isolated from *Irf8*$^{Gfp}$/*Cish*$^{-/-}$ mice that had been challenged with B16-GM tumors for 9 days compared to those isolated from similarly treated *Irf8*$^{Gfp}$/WT mice (Fig. 5C). We next investigated whether attenuation of JAK/STAT signaling could rescue *Irf8* transcription in *Cish*$^{-/-}$ GM-MØs. *Irf8*$^{Gfp}$/*Cish*$^{-/-}$ BM progenitors were cultured in the presence of GM-CSF with/without the addition of RUXO on Day 5 of culture. On Day 7, we noted that the *Irf8*$^{Gfp}$/*Cish*$^{-/-}$ GM-MØs treated with RUXO exhibited higher IRF8-GFP expression than the untreated *Cish*$^{-/-}$ GM-MØs (Fig. 5D). Similar observations were made for GM-DCs (Fig. 5D). These results suggest that the sustained JAK/STAT5 activation observed in *Cish*$^{-/-}$ GM-MØs inhibits IRF8 expression.

We then explored whether the downregulation of IRF8 contributed to the impaired IL-12 production observed in *Cish*$^{-/-}$ GM-MØs. The first supporting evidence came from the experiment performed with *Irf8*$^{Gfp}$ reporter mouse, in which we found that IRF8-GFP$^{hi}$ GM-MØs produced significantly higher amounts of IL-12 than IRF8-GFP$^{lo}$ GM-MØs (Fig. 5E). We then tested whether a lack of IRF8 impacted the capacity of GM-MØs to produce IL-12. To circumvent the defective myelopoiesis observed in germline IRF8-KO mice [42], we used *CD11c-Cre/Irf8*$^{fl/fl}$ (IRF8cKO) mice to generate GM-MØs. In this system, the compartment of Ly6G$^{+}$ granulocytes was similar between WT and IRF8cKO mice, while that of GM-DCs were slightly reduced in IRF8cKO mice (Fig. 5F). Consistent with our earlier observations, GM-MØs derived from IRF8cKO mice exhibited reduced IL-12 production following CpG stimulation compared to their WT counterparts (Fig. 5F). IRF8cKO GM-MØs also showed increased expression of the M2 MØ marker Arg1 compared to WT GM-MØs. However, the phenotype of IRF8cKO GM-MØs was less pronounced than that of *Cish*$^{-/-}$ GM-MØs (Fig. 5G). Crucially, IRF8 overexpression in *Cish*$^{-/-}$ GM-MØs substantially increased IL-12 production following CpG stimulation, suggesting that the reduced Irf8 expression observed in *Cish*$^{-/-}$ GM-MØs impaired their capacity to produce IL-12 (Fig. 5H). Collectively, our data suggest that CIS deficiency leads to increased STAT5 activation, resulting in the downregulation of IRF8 and hindering GM-MØ polarization into M1-like MØs.

**IRF8 regulates the gene program involved in MØ polarization**

Our results point to a critical role for CIS in maintaining an adequate IRF8 concentration, which ultimately controls MØ polarization. To gain insight into the potential instructive role of IRF8 regulation in controlling GM-MØ polarization, we performed CUT&Tag sequencing [43] to identify the genes directly targeted by IRF8 in GM-MØs. To facilitate our pull-down strategy, we derived GM-MØs from *Irf8*$^{Gfp}$/WT and *Irf8*$^{Gfp}$/*Cish*$^{-/-}$ mice, in which IRF8 is expressed as a fusion protein with GFP, and the pull-down step was performed with an anti-GFP Ab (Fig. S6A and B). Using this strategy, we identified 12,142 binding sites occupied by IRF8 in the genome of WT GM-MØs and 10,270 binding sites in that of *Irf8*$^{Gfp}$/*Cish*$^{-/-}$ GM-MØs (Fig. 6A). Comparison of our genome-wide IRF8 binding dataset with our RNA-seq data allowed us to identify putative IRF8-regulated genes. For genes positively regulated by CIS (downregulated in *Cish*$^{-/-}$ GM-MØs), 34% of them displayed at least one IRF8 binding site, while for genes negatively regulated by CIS (upregulated in *Cish*$^{-/-}$ GM-MØs), 28% of them displayed at least one IRF8 binding site (Fig. 6B). As we reasoned that CIS deficiency in GM-MØs led to a perturbed polarization potential, in part due to the lack of IRF8 upregulation, we focused on the genes associated with MØ polarization (Supplemental Table 1). For M1 MØ-associated genes, 40% of the M1 MØ genes positively regulated by CIS (*Ace, Cd74* and *Cyyb*) were bound by IRF8, while only 3% of the M1 MØ genes negatively regulated by CIS (*Dusp6*) were bound by IRF8 (Fig. 6C). On the other hand, of the 56 M2 MØ signature genes bound by IRF8, 30% were negatively regulated by CIS (*Ahr, Chil4* and *Myc*), and 14% were positively regulated by CIS (*F13a1* and *Msr1*) (Fig. 6D). Taken together, these observations support that the CIS-mediated modulation of IRF8 plays a key role in the regulation of the M1-like state.

***Cish*$^{-/-}$ MØs increase the Th2 response and the severity of allergic asthma**

To determine if the M2-like MØ phenotype observed in the absence of CIS evoked a Th2 response in vivo, we transferred OVA-pulsed WT and *Cish*$^{-/-}$ GM-MØs into C57BL/6 mice and measured the production of IL-4 and IFN-γ by restimulated splenocytes after 6 days. IL-4 production was substantially increased in cells from mice that received OVA-pulsed *Cish*$^{-/-}$ GM-MØs compared to those from mice immunized with OVA-pulsed WT GM-MØs, while IFN-γ levels were reduced (Fig. 7A). Ex vivo evaluation of OVA-stimulated CD4$^{+}$ T cells confirmed that *Cish*$^{-/-}$ GM-MØs induced more IL-4-producing cells (Fig. 7B). Next, we compared the impacts of transferred OVA-pulsed GM-MØs of WT or *Cish*$^{-/-}$ origin on the induction of Th2 allergic inflammation [44]. To this end, we immunized WT mice with OVA-pulsed WT or *Cish*$^{-/-}$ MØs and then challenged them with nebulized OVA 4 weeks later (Fig. 7C). Following the challenge, the lungs of mice that were preimmunized with OVA-pulsed *Cish*$^{-/-}$ MØs contained significantly increased immune infiltrates compared to those of mice that received OVA-pulsed WT MØs (Fig. 7D). These immune infiltrates were accompanied by an increased prevalence of PAS$^{+}$ mucus-producing cells, enhanced lung tissue inflammation intensity and pronounced increases in the concentrations of a wide array of cytokines in the bronchoalveolar lavage fluid (BALF) in mice preimmunized with OVA-pulsed *Cish*$^{-/-}$ MØs (Fig. 7E–G). Notably, the IL-4:IFN-γ ratio from the same samples was calculated to reflect a Th2 bias, and the BALF of mice immunized with OVA-pulsed *Cish*$^{-/-}$ MØs preferentially contained increased levels of the Th2 cytokine IL-4 (Fig. 7H). Taken together, these data suggested that CIS deficiency resulted in the polarization of MØs featuring a strong capacity to induce a robust Th2 response that exacerbated the allergic asthma response. Thus, CIS modulated Th differentiation through control of MØ polarization independent of the reported cell-intrinsic role of CIS in controlling T-cell polarization [45].

## DISCUSSION

A central finding from our study is that CIS has a marked impact on GM-CSF-induced MØ polarization. In its absence and in microenvironments where GM-CSF was abundant, MØs became immunosuppressive, producing less IL-12, which ultimately resulted in the induction of a Th2 immune response. In contrast to IL-4-induced M2 polarization, which depends on the STAT6/IRF4 signaling axis [46], CIS deficiency induced M2-like MØ polarization following GM-CSF exposure through sustained activation of STAT5 and consequent downregulation of IRF8. Thus, we propose that CIS activity may represent a key intrinsic regulatory mechanism responsible for the functional polarization of MØs.

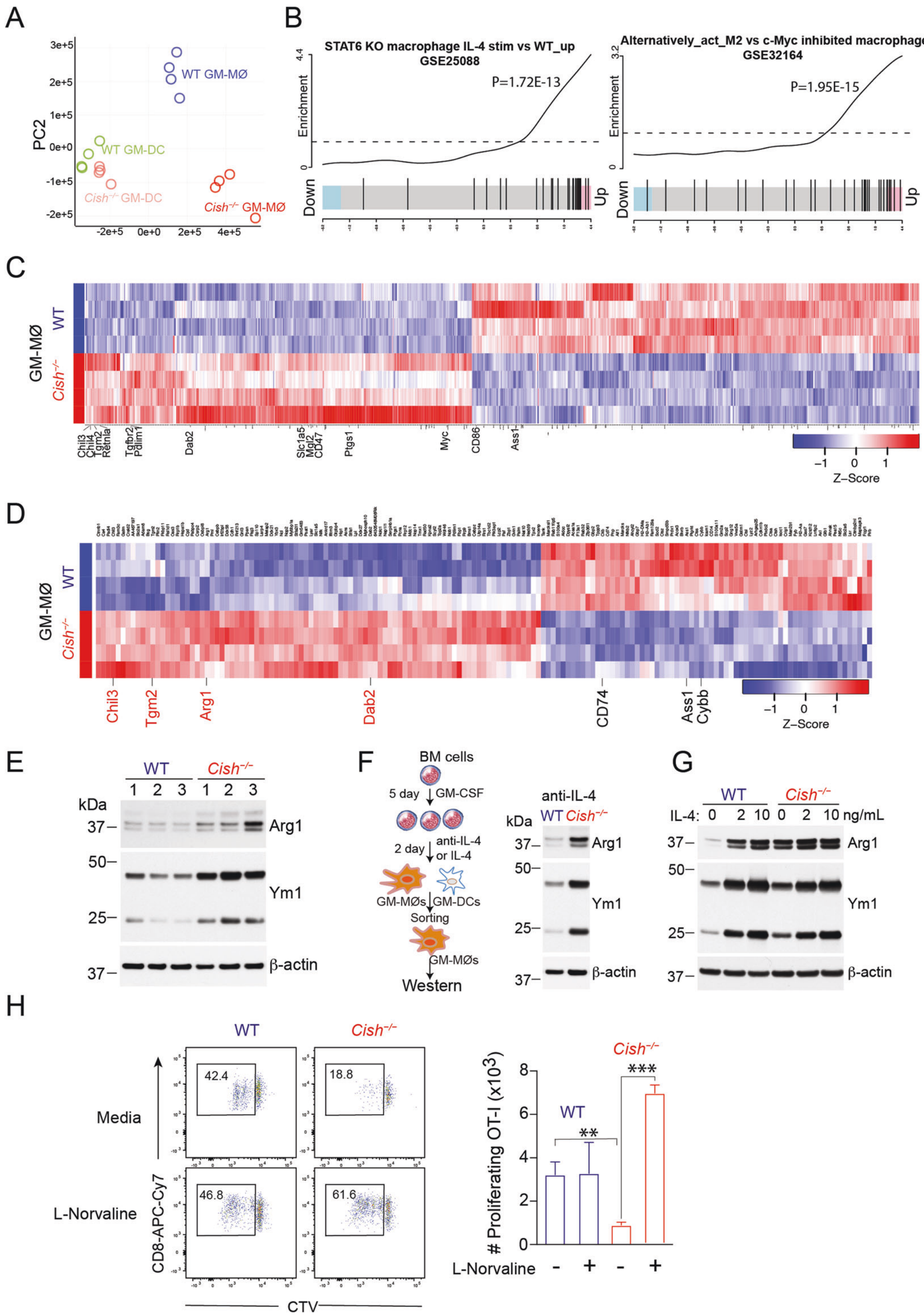


**Fig. 3** Cish−/− MØs display characteristics of M2 MØs. **A–C** RNA-seq analysis of WT and *Cish*$^{-/-}$ GM-MØs and GM-DCs. **A** Principal component analysis (PCA) plot of TPM values over dimensions 1 and 2 with samples from 4 individual mice per group colored by group for GM-MØs and GM-DCs. **B** Gene set enrichment analysis barcode plot comparing the expression of upregulated genes in *Cish*$^{-/-}$ GM-MØs with two previously reported M2 MØ signature gene sets. **C** Heatmap showing DEGs, with M2 MØ signature genes indicated in red ($log_2FC>X$, FDR < 0.05). **D** Proteomic analysis of GM-MØs derived from 4 individual WT and *Cish*$^{-/-}$ mice. Heatmap showing the expression of differentially regulated proteins by the two types of GM-MØs, with M2 proteins indicated in red ($log_2FC > 0.6$, FDR<0.05). **E** Western blot analysis of Arg1 and Ym1 in WT or *Cish*$^{-/-}$ GM-MØs derived from 3 individual donors. **F, G** BM cells were cultured with GM-CSF for 5 days, and an anti-IL-4 antibody or recombinant IL-4 was then added. After 2 days, GM-MØs were sorted and analyzed for Arg1 and Ym1 expression by Western blotting. **F** Cultures ± anti-IL-4 antibody. **G** Cultures ± recombinant IL-4. **H** CTV-labeled OT-1 $CD8^+$ T cells were cocultured with GM-MØs and stimulated with OVA ± 12 mM L-norvaline. Dot plots show the OVA-stimulated proliferation of CTV-labeled $CD8^+$ T cells. Bar graphs show the numbers of proliferating $CD8^+$ T cells. *$P < 0.05$, **$P < 0.01$, **$P < 0.001$; multiple-group ANOVA

At the cellular level, the development of proinflammatory M1-like MØs in vitro upon GM-CSF stimulation has been documented for both humans and mice [3, 5]. Similarly, in murine models of autoimmunity, GM-CSF has been shown to promote MØ pathogenicity associated with the production of proinflammatory cytokines [47, 48]. However, GM-CSF has also been associated with the development of suppressive M2-like MØs in various settings [11, 12, 16]. How GM-CSF drives these contrasting cellular fates of MØs is still largely unknown. A simple interpretation of the dichotomy of MØ polarization under GM-CSF stimulation is a model of ligand abundance-mediated polarization, as the development of suppressive M2-like MØs is largely associated with high levels of GM-CSF [11, 12]. At the molecular level, heightened STAT5 activation under GM-CSF stimulation has been linked to the development of M2-like MØs [12, 49]. Accordingly, neutralization of GM-CSF or STAT5 inhibition can reverse M2 MØ polarization [50]. Our study identified another layer of control independent of GM-CSF abundance. Here, we report that CIS acts as a cell-intrinsic rheostat in controlling STAT5 activation independent of the activation of PI3K or MAPK. CIS deficiency in GM-MØs led to heightened and sustained STAT5 activation that favored M2-like MØ differentiation. Fittingly, attenuation of upstream signaling with a JAK inhibitor increased IL-12 production and reduced the expression of Arg1 and Ym1 in *Cish*$^{-/-}$ MØs.

Here, we revealed the CIS-modulated GM-CSF/STAT5/IRF8 signaling axis that acts in MØ polarization regulation. In our study, GM-CSF signaling in *Cish*$^{-/-}$ MØs resulted in suboptimal expression of IRF8, in part due to the hyperactivation of STAT5. Accordingly, JAK inhibition in *Cish*$^{-/-}$ MØs prevented STAT5 phosphorylation and restored normal IRF8 expression. STAT5 activation has been shown to suppress the induction of *Irf8* transcription in plasmacytoid DCs [51]. IRF8 has also been reported to be a critical positive regulator of IL-12 expression [52, 53]. This strongly indicates that *Irf8* downregulation is functionally linked to the reduced IL-12 production in *Cish*$^{-/-}$ MØs. Earlier studies provided circumstantial evidence supporting the idea that downregulation/silencing of IRF8 could represent a defining event favoring the development of M2-like MØs through increased expression of M2 MØ genes [54–56]. Our study demonstrated the extent of IRF8 binding in MØs, particularly in the vicinity of many genes that have been associated with MØ polarization, suggesting a critical instructive role in driving MØ polarization. Despite its importance, the downmodulation of IRF8 is unlikely to be the sole downstream event of the GM-CSF/STAT5 pathway that leads to M2 MØ polarization in *Cish*$^{-/-}$ MØs, although the identity of any other contributing signaling pathways will require future studies.

Although M2-like MØs are known to promote Th2-cell differentiation [15], the molecular mechanisms responsible for this process are not well understood. It has previously been reported that the M2 MØ signature genes Ym1/2 can directly influence Th2-cell development [57, 58]. Our transcriptomic and proteomic approaches highlighted the elevated expression of TGM2, Arg1 and FIZZ1 in *Cish*$^{-/-}$ GM-MØs (Fig. 3), all of which have been shown to play roles in allergic asthma [59]. Thus, we contend that CIS expression in myeloid cells has a prominent role in regulating Th2 immunity, independent of the reported role for CIS in T cells involved in promoting Th2-cell differentiation [45].

Overall, we reveal that CIS acts as a brake on GM-CSF signaling and is critical for MØ polarization. Through dissection of the molecular and functional nature of *Cish*$^{-/-}$ GM-MØs, we provide significant insights into how GM-CSF can shape MØ polarization. We argue that CIS expression in myeloid cells may be beneficial in allergic responses and antitumor immunity by curtailing GM-CSF signaling to prevent M2 MØ polarization and pathogenic Th2 responses.

## MATERIALS AND METHODS

### Mice

Mice were housed under specific pathogen-free conditions at The Walter & Eliza Hall Institute of Medical Research. The strains are listed in Supplementary Table 4. *Cish*$^{-/-}$ mice were kindly provided by J. Ihle and E. Parganas (St. Jude Children's Research Hospital). Chimeric mice were from the F1 generation (Ly5.1/Ly5.2); these recipients were irradiated with 2 doses of 550 rads and reconstituted with $2 \times 10^6$ BM cells from Ly5.1 and *Cish*$^{-/-}$ mice. All experiments were performed following relevant guidelines and regulations approved by the Walter & Eliza Hall Institute of Medical Research animal ethics committee (Projects #2016.014, #2017.008, and #2018.040).

### Cell preparation, antibodies, and flow cytometry

Cells were isolated from the spleen, lungs and tumors by digestion in collagenase/DNase I. The antibodies used in this study are listed in Supplementary Table 4. Cell numbers were determined by the addition of fluorochrome-conjugated calibration beads (BD Biosciences, San Jose, CA) directly to the samples. To evaluate expression levels, a fluorescence minus one (FMO) control was included. Data were collected using a FACSVerse (BD Biosciences) and analyzed using FlowJo software (Tree Star, Ashland, OR). Cell sorting was performed using a FACSAria or an Influx cell sorter (BD Biosciences).

### BM cell culture

BM cells from mice were isolated by flushing femurs and tibias with 5 ml PBS supplemented with 2% heat-inactivated fetal bovine serum (FBS) (Sigma Aldrich, Lenexa, KS, USA). The BM cells were centrifuged once and then resuspended in tris-ammonium chloride at 37 °C for 30 s to lyse red blood cells. The cells were centrifuged again and then strained through a 70-μm filter before being resuspended in RPMI-1640 medium supplemented with 10% FBS. For GM-CSF-stimulated cultures, BM cells were resuspended at $0.5 \times 10^6$/ml in medium containing titrated doses of GM-CSF in 12-well plates. After 3–4 days, fresh medium with cytokines was added to the cultures. Cell cultures were maintained for up to 7 days. For further analysis, MØs and DCs were sorted on a FACSAria (BD Biosciences).

### T-cell proliferation assays

$CD4^+$ T cells (OT-II) and $CD8^+$ T cells (OT-I) were purified from TCR-transgenic mice by sorting and labeled with CTV (Invitrogen, Thermo Fisher, Waltham; MA) according to the manufacturer's protocol. Labeled cells were cultured at $1 \times 10^5$ cells in 200 μL RPMI-1640 medium supplemented with 10% FBS in flat-bottom 96-well plates in the absence or presence of antigen-presenting cells and defined antigens. The cell cultures were harvested 3 days later. T-cell proliferation was evaluated by monitoring CTV dilution. The arginase inhibitor 1 L-norvaline (12 mM, Sigma–Aldrich) was included in some cultures. The cytokine levels in culture supernatants were analyzed using a BioPlex kit (Bio-Rad). In some experiments, CTV-labeled $CD8^+$ T cells were also stimulated with 5 μg/ml anti-CD3 and 2 μg/ml anti-CD28 for 3 days. Cell proliferation and cytokine production were evaluated as described above.

### Antigen uptake and processing

For antigen uptake, $1 \times 10^6$ cells were incubated with 100 μg/mL FITC-OVA at 37 °C or kept on ice for 30 min. For antigen processing, $1 \times 10^6$ cells were incubated with 100 μg/mL DQ-OVA (ThermoFisher) at 37 °C for 30 min. Then, the samples were either incubated at 37 °C for an additional 90 min or kept on ice. After the incubation, the cells were washed with cold PBS containing 2% FBS-EDTA (0.02 mM) and analyzed by flow cytometry.

### Cell signaling analysis by immunoblotting

GM-MØs were isolated by FACS sorting. The purity of enriched cells was consistently >95%. For cell signaling assessment, cells were washed free of GM-CSF, rested for 4 h and then restimulated in vitro with recombinant GM-CSF (50 ng/ml) for the indicated times in RPMI-1640 medium supplemented with antibiotics and 10% heat-inactivated FBS. The cells were washed in cold PBS and pelleted, followed by lysis. Approximately $5 \times 10^5$ sorted cells were collected per sample and lysed in 100 μl lysis buffer (50 mM Tris-HCl, pH 7.4; 150 mM NaCl; 0.25% deoxycholic acid; 1% NP-40; and 1 mM EDTA) supplemented with protease inhibitors (Complete Cocktail tablets, Roche), 1 mM PMSF, 1 mM $Na_3VO_4$ and 1 mM NaF for 30 min on ice. The lysates were clarified by centrifugation at 13,000 rpm for 15 min at 4 °C. Gel electrophoresis was carried out with 4–12% NuPAGE Bis-Tris gels, followed

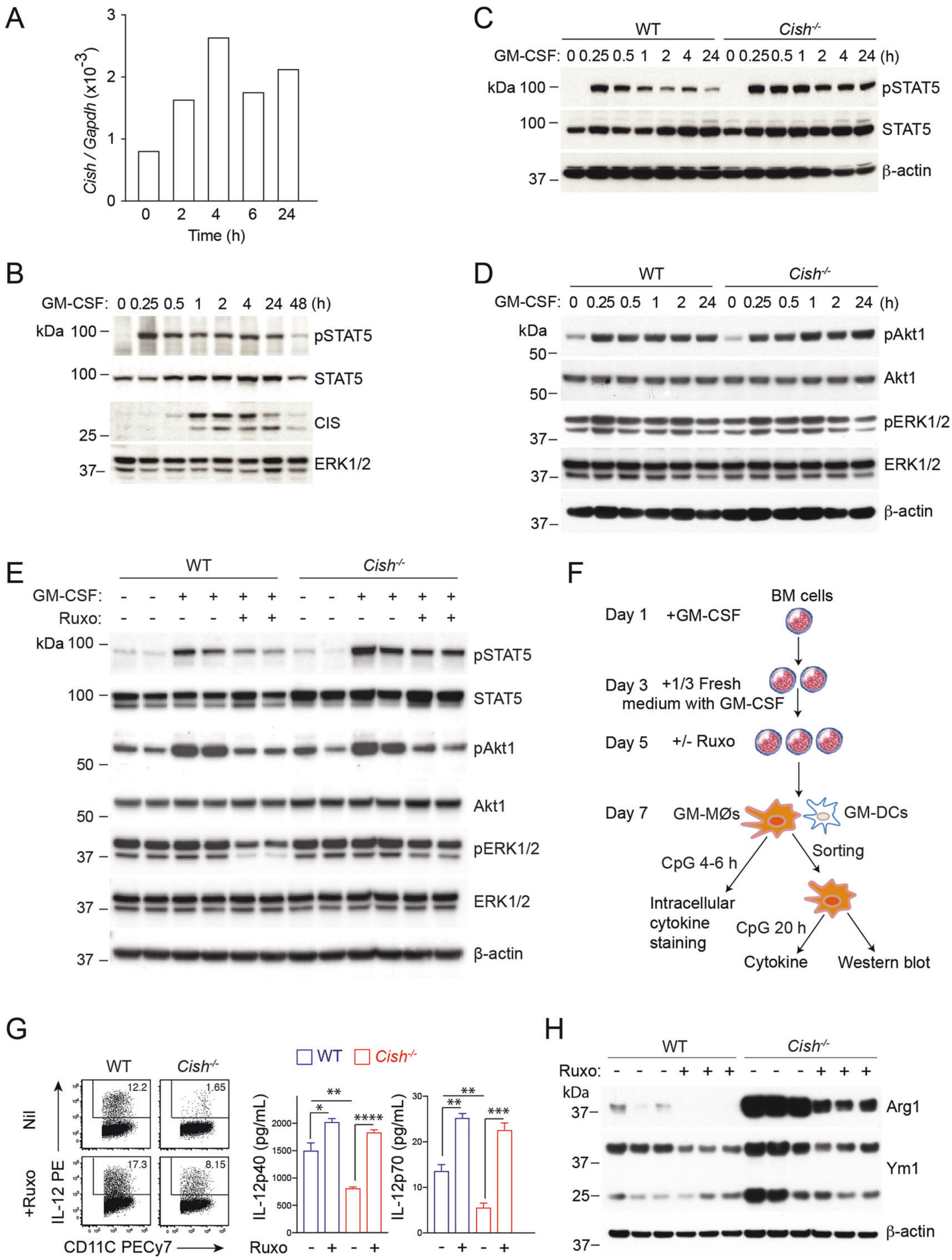


**Fig. 4** Cish−/− GM-MØs have enhanced STAT5 activation, contributing to an M2-like phenotype. **A**, **B** Purified GM-MØs, generated on Day 7 in the presence of GM-CSF, were restimulated in vitro with recombinant GM-CSF (50 ng/ml) for the indicated times. **A** The induction of *Cish* mRNA expression relative to that of the housekeeping gene *Gapdh* in GM-MØs upon GM-CSF stimulation was determined by RT–qPCR analysis of extracted RNA samples. **B** The induction of CIS protein expression and STAT5 activation in GM-MØs upon GM-CSF restimulation were determined by immunoblotting. **C**, **D** Purified WT and *Cish*$^{-/-}$ GM-MØs, generated on Day 7 in the presence of GM-CSF, were stimulated in vitro with recombinant GM-CSF (50 ng/ml) for the indicated times. Cell lysates were analyzed by western blotting to assess (**C**) STAT5 activation and (**D**) Akt1 and ERK 1/2 activation. **E** BM cells from WT or *Cish*$^{-/-}$ mice were cultured with GM-CSF for 5 days. GM-MØs were harvested and stimulated ± GM-CSF (50 ng/ml) or the JAK inhibitor ruxolitnib (Ruxo) (0.2 μM) for 4 h. The cells were lysed for Western blotting to assess STAT5, Akt1 and ERK1/2 activation. Data were derived from 2 individual mice. **F-G** BM cells were cultured with GM-CSF for 5 days and supplemented ± RUXO (0.2 μM) for 2 days. **G** The IL-12 production of GM-MØs upon CpG stimulation was evaluated by intracellular cytokine staining and secretion. *$P < 0.05$, **$P < 0.01$, ***$P < 0.001$, ****$P < 0.0001$; multiple-group ANOVA. Data are representative of two independent experiments. **H** Purified WT and *Cish*$^{-/-}$ GM-MØs were analyzed for Ym1 and Arg1 expression by western blotting. In each western blot, β-actin was used as a loading control, with the exception of (**B**), in which ERK1/2 was used as the loading control. Data were derived from 3 individual mice

by transfer to nitrocellulose membranes (Amersham) and immunoblotting. The primary antibodies are listed in Supplementary Table 4.

## Cell stimulation and cytokine assay

MØs and moDCs derived from 7-day BM cultures were purified by sorting. Then, the cells were cultured at $5 \times 10^4$ cells in 200 µl RPMI-1640 medium supplemented with 10% FBS in U-bottom 96-well plates in the absence or presence of LPS (1 µg/mL, Sigma), CpG ODN 1668 (1 µM, InvivoGen), an agonistic anti-CD40 Ab (5 µg/ml, clone FGK4.5) or PolyI:C (5 µg/ml, InvivoGen) for 20 h. For detection of cytokines in supernatants in in vitro assays, the indicated cytokines were detected using a BioPlex kit (Bio-Rad) or ELISA kit (Invitrogen) following the manufacturer's instructions. For intracellular cytokine staining, cells were stimulated for 4–6 h with 0.5 µM CpG or 50 ng/ml PMA/1 mM ionomycin with GolgiStop (BD Biosciences), stained for cell-surface markers, fixed/permeabilized using a Cytofix/Cytoperm kit (BD Biosciences), and stained with anti-cytokine antibodies. The antibodies are listed in Supplementary Table 4.

## JAK inhibition and IL-4 neutralization during in vitro MØ differentiation

For JAK inhibition, BM cells were cultured at $0.5 \times 10^6$ cells/ml in medium containing 10 ng/mL GM-CSF in 12-well plates for 5 days. Ruxolitinib (RUXO) (0.2 µM, Invitrogen) was added, and the cells were harvested on Day 7. For IL-4 neutralization, BM cells were cultured at $0.5 \times 10^6$ cells/ml in medium containing 10 ng/mL GM-CSF in 12-well plates in the presence of an anti-IL-4 antibody (50 µg/ml, clone 11B11) for 7 days.

## Tumor induction

A total of $1–5 \times 10^5$ GM-CSF-transduced mouse melanoma B16F10 cells (B16-GM cells, provided by Prof. Jose Villadangos with permission from Prof Glenn Dranoff [8]) were injected s.c. into the flank of test mice. The mice were evaluated after 1–2 weeks.

## RNA sequencing

GM-DCs and GM-MØs from 4 individual mice were enriched by sorting. RNA was isolated independently from biological replicates with RNeasyPlus Mini kits (Qiagen). mRNA reverse transcription and cDNA libraries were prepared using a TruSeq RNA Sample preparation kit (Illumina) following the manufacturer's instructions. Samples were sequenced with an Illumina NextSeq 500 sequencing system, producing between 14–20 x$10^7$ single-end 85-bp reads per sample.

## Bioinformatic analysis of RNA-seq data

RNA-seq reads were quantified against the Ensembl [60] v31 GRCm38 transcriptome using Kallisto [61]. Differential expression analysis was conducted using Sleuth [62] at the gene level via the method of Pimentel et al. [63]. Q-values were calculated using the Benjamini–Hochberg [64] adjustment, and log-fold changes at the gene level were estimated by combining transcript level abundances normalized to transcripts per million reads (TPM) [65]. Heatmaps of TPM expression values were plotted with the coolmap function of the limma package [66].

## Sample preparation for mass spectrometry-based proteomics

GM-MØs (1–1.5 x $10^6$ cells/replicate) from 4 individual WT or *Cish*$^{-/-}$ mice were sorted on a FACSAria to achieve a final purity of 99–100%. The cells were washed three times with ice-cold PBS prior to dry cell pellet storage at −80 °C. The cells were lysed in preheated (95 °C) 5% SDS/10 mM Tris/10 mM Tris (2-carboxyethyl) phosphine/5.5 mM 2-chloroacetamide and heated at 95 °C for 10 min. Neat trifluoracetic acid (Sigma–Aldrich) was added to hydrolyze the DNA, resulting in a final concentration of 1%. The lysates were quenched with 4 M Tris (pH 10), resulting in a final concentration of ~140 mM Tris (pH 7). The myeloid cell protein lysates (~50 µg) were prepared for mass spectrometry (MS) analysis as previously described [67]. Acidified peptide mixtures were analyzed by nanoflow reversed-phase liquid chromatography–tandem mass spectrometry (LC–MS/MS) on an Easy-nLC 1000 system (Thermo Fisher Scientific) coupled to a Q-Exactive HF (QE-HF) mass spectrometer equipped with a nanoelectrospray ion source and in-source column heater (Sonation) at 40 °C for automated MS/MS (Thermo Fisher Scientific). The peptide mixtures were loaded in buffer A (0.1% formic acid, 2% acetonitrile, and Milli-Q water) and separated by reverse-phase chromatography using a $C_{18}$ fused silica column (packed emitter, internal diameter: 75 µm, outer diameter: 360 µm × 25 cm length, IonOpticks) using flow rates and data-dependent methods previously described [25]. Raw files consisting of high-resolution MS/MS spectra were processed with MaxQuant (version 1.5.8.30) for feature detection and protein identification using the Andromeda search engine as previously described [67]. LFQ quantification was selected, with a minimum ratio count of 2. PSM and protein identifications were filtered using a target-decoy approach at an FDR of 1%. Only unique and razor peptides were considered for quantification, with intensity values present in at least 2 out of the 3 replicates per group. Statistical analyses were performed using LFQAnalyst (https://bioinformatics.erc.monash.edu/apps/LFQ-Analyst/), whereby the LFQ intensity values were used for protein quantification. Missing values were replaced by values drawn from a normal distribution of 1.8 standard deviations and a width of 0.3 for each sample (Perseus-type). Proteinwise linear models combined with empirical Bayes statistics were used for differential expression analysis using the Bioconductor package limma, whereby the adjusted *p* value cutoff was set at 0.05 and the log2-fold change cutoff was set at 1. The Benjamini–Hochberg (BH) method for FDR correction was used.

## CRISPR/CAS9-mediated deletion of *CISH* in human CD34$^+$ cord blood cells

CD34$^+$ cells were isolated from human cord blood (Stemcell Technologies) and cultured for 2 days in expansion medium (Miltenyi). CIS RNPs were assembled by incubating 1 ml of 30 mM *CISH* gRNA (5′-CTCACCAGATTCCC-GAAGGT-3′; Synthego), 1.7 ml of 67 nM Cas9 (Integrated DNA Technologies), 1 ml of electroporation enhancer (Integrated DNA Technologies) and 1.3 ml of PBS for 10 min at room temperature. A total of $5 \times 10^5$ cells were pelleted, resuspended in RNP solution and 20 ml of primary cell P3 buffer (Lonza) and transferred to an electroporation cuvette (Lonza). The cells were electroporated using a 4D-Nucleofector (Lonza) with pulse code CM-137 and rested in complete medium for 10 min before being transferred to a cell culture dish. The cells were cultured with 5 ng/mL huGM-CSF (R&D) for 7 days. A small pellet of cells was collected for sequencing to determine the CIS indel frequency.

## Cell transfer

WT and *Cish*$^{-/-}$ GM-MØs were incubated with 10 mg/ml OVA in serum-free medium at 37 °C for 30 min. After washing with cold PBS, OVA-pulsed WT and *Cish*$^{-/-}$ GM-MØs were injected i.v. into B6 mice or *Rag1−/−Il2rg−/−* mice infused with $10^6$ Ly5.1-OT-1 cells 2 weeks prior. OT-1 cell expansion was evaluated 3–7 days after GM-MØ injection.

## CUT&Tag sequencing

CUT&Tag was performed with the Hyperactive in situ ChIP Library Prep Kit (Vazyme) following the manufacturer's recommendations. Briefly, *Cish*$^{-/-}$ GM-MØs were sorted from GM-CSF-supplemented cultures of BM cells isolated from WT *Irf8*$^{Gfp}$ or *Cish*$^{-/-}$ *Irf8*$^{Gfp}$ mice. GFP$^+$ GM-MØs ($1 \times 10^5$ cells) were bound to concanavalin A-coated magnetic beads (Bags laboratories) and subjected to immunoprecipitation with 0.5 µg of primary antibody (rabbit anti-GFP, ab290; rabbit anti-H3K27me3, CST: 9733; or rabbit anti-mouse IgG control). Following the primary antibody incubation and washing using a magnetic stand, a secondary anti-rabbit antibody was added and incubated under gentle agitation for 1 h (Antibodies online ABIN101961). The cells were washed and incubated for 1 h in a mix of Hyperactive pG-Tn5/pA-Tn5 Transposon with Dig-300 Buffer at a final concentration of 0.04 µM. Excess reagents were washed out using the magnetic stand, and the cells were resuspended in 100 µl of Tagmentation buffer and incubated at 37 °C for 1 h. The reaction was stopped by heat inactivation (55 °C for 10 min). DNA was purified using Ampure XP beads (Beckman Coulter). For library amplification, 24 µl of DNA was mixed with 10 µl of 5x TAB, 1 µl of TAE, and 5 µl of uniquely barcoded i5 and i7 primers [68] and amplified for 14 cycles (72 °C for 5 min; 98 °C for 30 s; 14 cycles of 98 °C for 10 s, 63 °C for 10 s and 72 °C for 1 min; and hold at 4 °C). The PCR products were purified with Ampure XP beads and eluted in 25 µl of water. The eluted DNA was checked for region molarity via a high-sensitivity D5000 TapeStation (Fig. S6B). The libraries were sequenced on an Illumina NextSeq platform, and 150-bp paired-end reads were generated.

## CUT&Tag data analysis

Raw data were uploaded to the Galaxy Australia website (https://usegalaxy.org.au/). The sequence quality was checked via FastQC and MultiQC. Then, the raw data were aligned to mm10 via Bowtie2 version

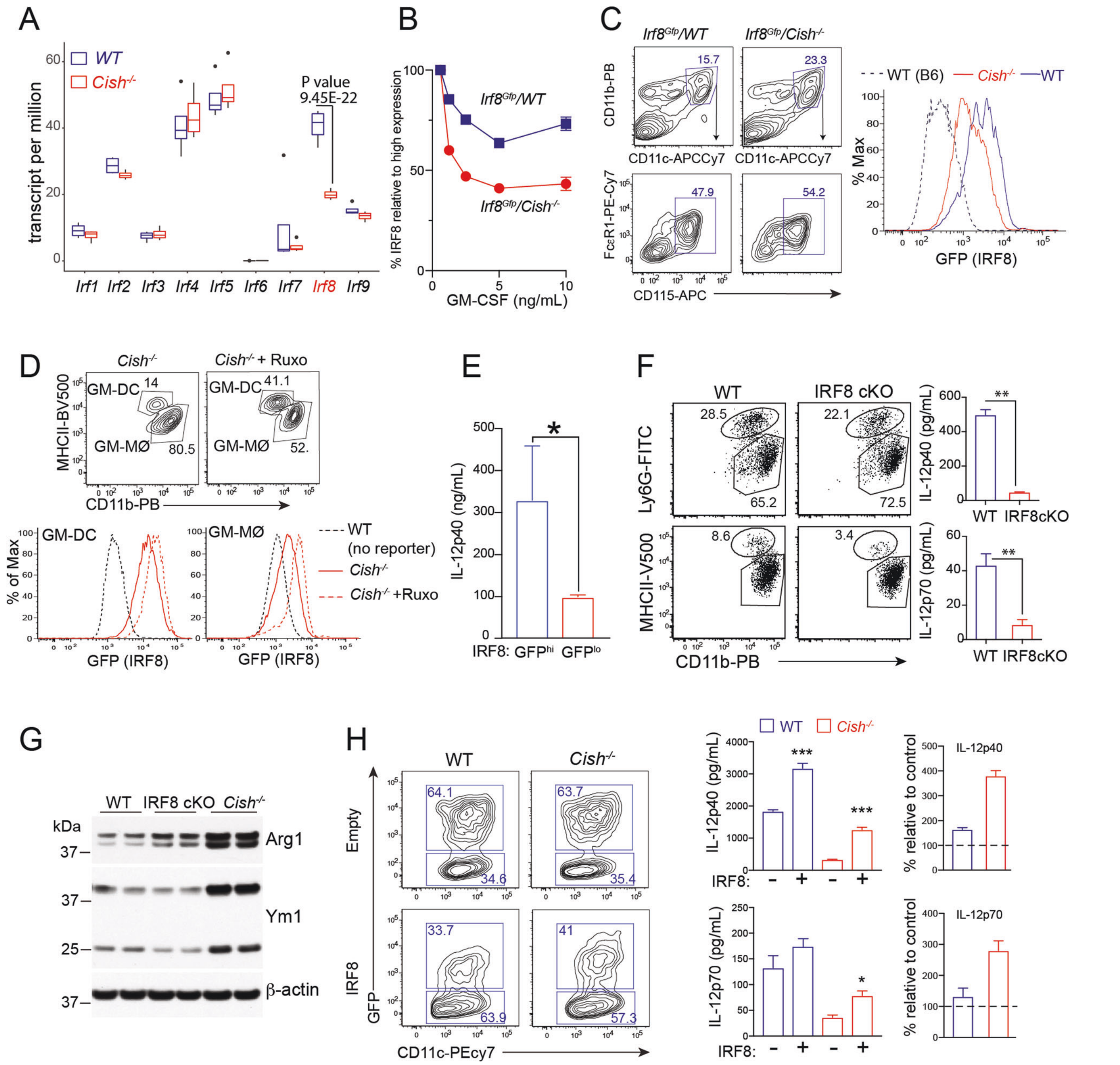

**Fig. 5** Cish−/− MØs have reduced expression of IRF8, resulting in an M2-like phenotype. **A** Interferon regulatory factor (IRF) expression in WT and *Cish*$^{-/-}$ GM-MØs was analyzed by RNA-seq. Boxplot showing IRF expression in WT and *Cish*$^{-/-}$ GM-MØs ($n = 4$). **B** BM cells from *Irg8*$^{Gfp}$ mice ± *Cish* deficiency were cultured with different concentrations of GM-CSF. Heatmap showing the MFI of *Irf8*$^{Gfp}$ in GM-MØs. **C** *Irf8*$^{Gfp}$ mice ± *Cish* deficiency were engrafted with B16-GM cells. Isolated spleen MØs were evaluated for the expression of IRF8-GFP. Negative controls (dotted line) were MØs from B6 mice. **D** *Irf8*$^{Gfp}$/*Cish*$^{-/-}$ BM cells were cultured in the presence of GM-CSF for 5 days. The cells were then cultured with RUXO for an additional 2 days, and IRF8-GFP expression by GM-MØs and GM-DCs was evaluated. **E** GM-MØs from *Irf8*$^{Gfp}$ mice were sorted into IRF8-GFP$^{hi}$ (top 50%) and IRF8-GFP$^{lo}$ (bottom 50%) populations. The sorted GM-MØs were then stimulated with CpG for 20 h, and the IL-12 concentration in the culture supernatant was measured by ELISA. *$P < 0.05$, Student's *t* test. **F**, **G** GM-MØs from *CD11c-cre-IRF8*$^{fl/fl}$ (IRF8cKO) and WT mice were stimulated with CpG for 20 h. **F** IL-12 production was then measured by ELISA. **$P < 0.01$, Student's *t* test. **G** Sorted GM-MØs cultured from BM cells isolated from IRF8cKO, WT or *Cish*$^{-/-}$ mice were also analyzed for the expression of Arg1 and Ym1 by western blotting. **H** BM progenitor cells from WT and *Cish*$^{-/-}$ mice were transduced with either an empty/GFP- or IRF8/GFP-encoding retrovirus and cultured with 10 ng/ml GM-CSF for 5 days. The gated population represents the frequency of transduced (GFP$^+$) GM-MØs. Sorted transduced GM-MØs were stimulated with CpG for 20 h. The IL-12 concentration in the culture supernatant is presented in bar graphs. The right panels show the % increase in IL-12 production by cells transduced with the IRF8/GFP-encoding vector relative to that of cells of the same genotype transduced with the empty/GFP-encoding vector. Data are representative of 3 independent experiments. *$P < 0.05$, ***$P < 0.001$; multiple-group ANOVA

2.3.4.3 with the following options: --local --very-sensitive-local --no-unal --no-mixed --no-discordant -- phred33 -I 10 -X 700 [69, 70]. Duplicate reads were removed via a SAM/BAM filter. The biological duplicate sample reads were pooled together via the Merge BAM files package. Then, peaks were called via MACS2 (q < 0.01) [71, 72]. The binding peaks were viewed using the Integrated Genome Brower (IGB) [73]. The peaks were annotated via ChIPseeker [74]. The peak intersection between WT and *Cis*$^{-/-}$ GM-MØs was calculated via Bedtool [75].

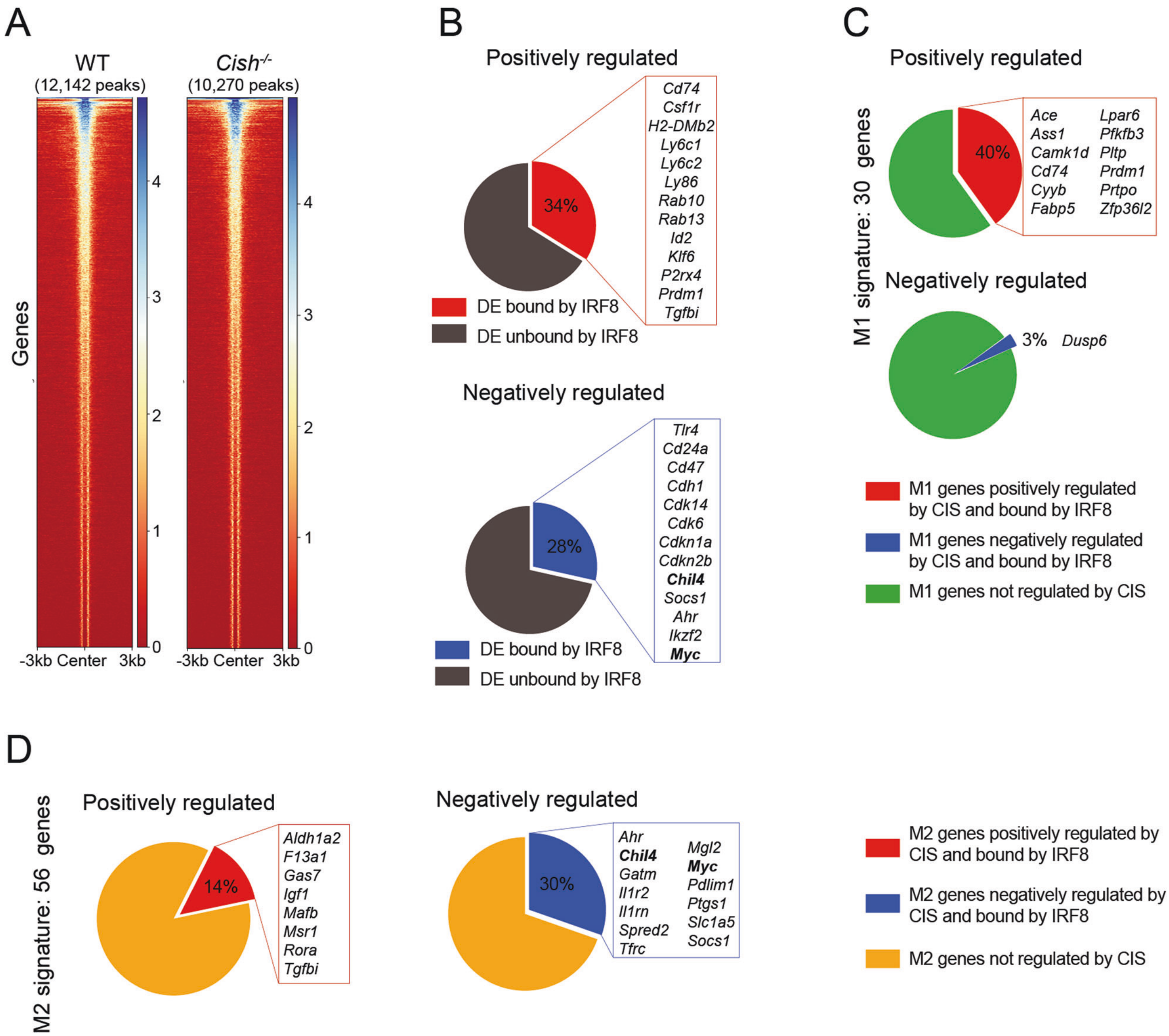


**Fig. 6** IRF8 regulates genes associated with MØ polarization. **A** Heatmap showing IRF8 binding in WT and *Cish*$^{-/-}$ GM-MØs. The number of IRF8 peaks identified for each genotype is shown. **B** Differentially expressed genes (DEGs) between WT and *Cish*$^{-/-}$ GM-MØs displaying at least one IRF8 binding site in the locus. Peaks were assigned to the closest gene. Top: genes positively regulated by CIS (downregulated in *Cish*$^{-/-}$ GM-MØs), bottom: genes negatively regulated by CIS (upregulated in *Cish*$^{-/-}$ GM-MØs). **C** M1 MØ-associated DEGs displaying an IRF8 binding site in the locus. Top: M1MØ-associated genes positively regulated by CIS, bottom: M1 MØ-associated genes negatively regulated by CIS. **D** M2 MØ-associated DEGs displaying an IRF8 binding site in the locus. Top: M2 MØ-associated genes positively regulated by CIS, bottom: M2 MØ-associated genes negatively regulated by CIS

### Retroviral transduction

Retroviral supernatants were generated by transient transfection of 293T cells with plasmids encoding viral envelope proteins (pMD1-gag-pol and pCAG-Eco) and the expression vector pMSCV-iresGFP or pMSCV-IRF8iresGFP using FuGeneHD (Promega). The retroviral supernatants were centrifuged onto RetroNectin (Takara)-coated plates for 45 min at 4000 rpm and 32 °C. Cells were then cultured with the virus in the presence of 4 µg/ml polybrene (Sigma–Aldrich) for 12 h.

### Cell imaging

In total, $2 \times 10^5$/ml cells were suspended in 100 µl PBS, stained using a 1:1000 dye mixture (CellTracker violet LysoTracker green and DAPI, from Thermo Fisher) at 37 °C for 15 min, washed twice in PBS and plated in 96-well PerkinElmer Cell Carrier plates for imaging with a Leica SP8 confocal microscope. The volume of each cell was calculated using Imaris 9.1.2 by applying a surface to each cell using the CellTracker violet channel. Images at higher resolution were acquired using the same microscopy settings and processed on a FIJI platform.

### Allergic asthma model

To establish an allergic asthma model, $5 \times 10^6$ WT or *Cish*$^{-/-}$ GM-MØs were generated, loaded with OVA and then injected into recipient mice on Day 0 and Day 7. The allergic response to OVA was induced as described previously [76].

### Statistical analysis

Statistical comparisons of the mean difference between two groups from independent experiments were made using a two-tailed Student's *t* test, and data for multiple groups, dose–response curves or time courses were analyzed using ANOVA. Analyses were performed with Prism v.5.0 software (GraphPad, San Diego, CA). $P < 0.05$ was considered statistically significant.

## DATA AVAILABILITY

The RNA-seq data have been deposited in the European Nucleotide Archive (ENA) under dataset identifier PRJEB40745. The mass spectrometry proteomic data have

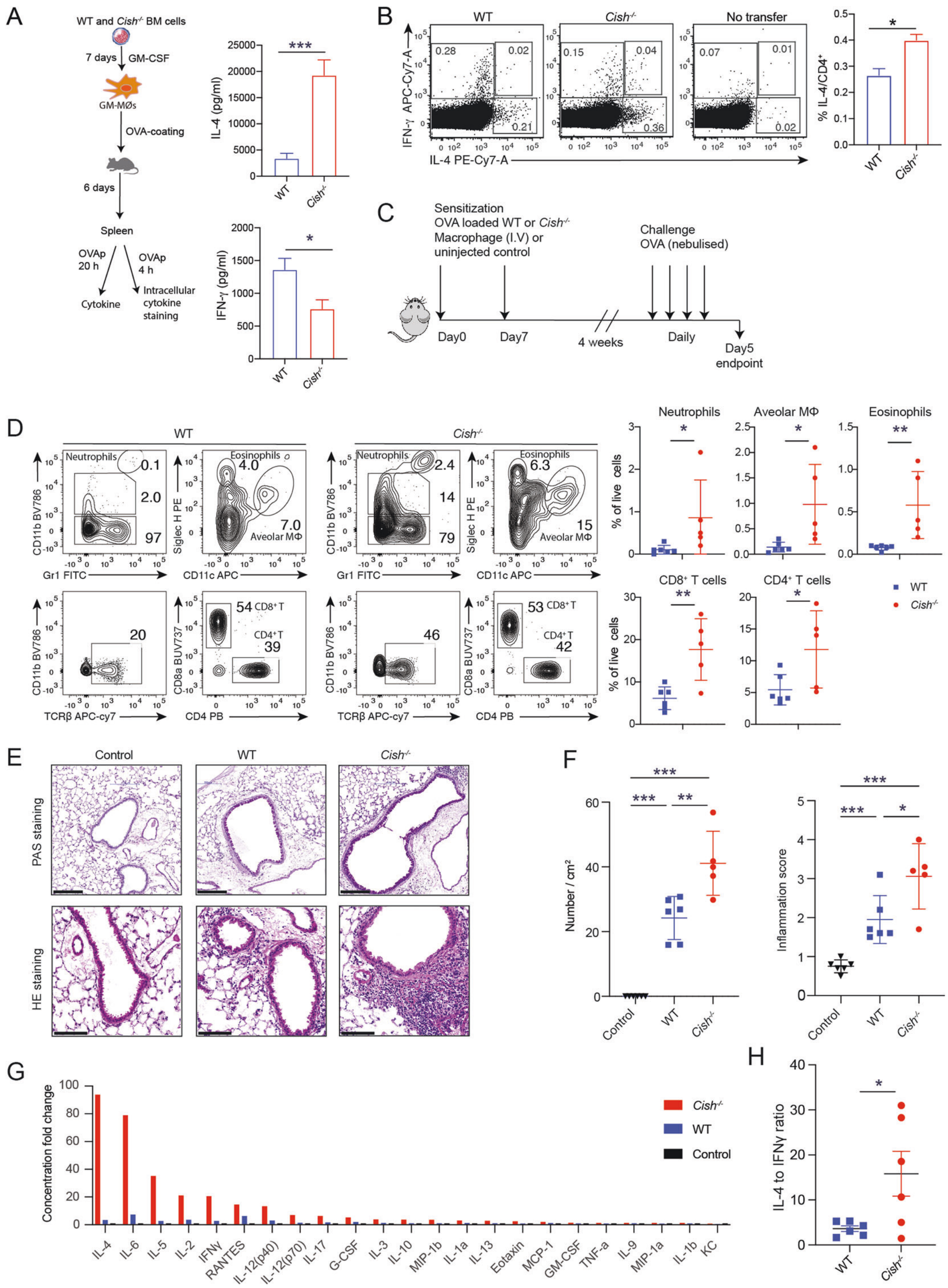


**Fig. 7** Cish-/- MØs promote Th2 responses and exacerbate allergic asthma. **A** Schematic showing the experimental approach for assessing the immune response induced by WT or *Cish*$^{-/-}$ GM-MØs. Six days after the transfer of OVA-coated GM-MØs, harvested spleen cells from 3 individual mice were cultured with OVA for 20 h. The supernatant was harvested for a cytokine assay. The bar graph shows the concentrations of IL-4, IFN-γ and IL-17A. **B** Spleen cells from mice treated as in (**A**) were pulsed with $OVA_{323-339}$ for 4 h. The proportions of IL-4- and IFN-γ-producing $CD4^+$ T cells were tested via intracellular staining. Dot plots show IL-4 and IFN-γ expression in $CD4^+$ T cells. The bar graph shows the percentage of $IL\text{-}4^+$ $CD4^+$ T cells. *$P < 0.05$, Student's *t* test. **C** Experimental protocol for OVA-induced inflammation. **D** Contour plots show the gating strategies for neutrophils, alveolar macrophages, eosinophils and T cells in the bronchoalveolar lavage fluid. Scatter plots show the mean ± SEM of different immune cell populations from individual mice treated as in (**C**). **E** Representative PAS and HE staining of the airways of mice treated as in (**C**). Scale bar = 200 µm. **F** Quantification of $PAS^+$ cells and the inflammation score. Bar graphs show the mean ± SEM of the indicated populations. Each dot represents one mouse. **G** The bronchoalveolar lavage fluid of mice treated as in (**C**) was analyzed for cytokine and chemokine expression by a BioPlex assay. The bar graph shows the fold change over the mean level in control mice. **H** Ratio of the IL-4 and IFN-γ concentrations in the same sample. Each dot represents one mouse. **$P < 0.01$, ***$P < 0.001$; Student's *t* test

been deposited in the ProteomeXchange Consortium via the PRIDE partner repository under the dataset identifier PXD018390 (reviewer token: Username: reviewer98346@ebi.ac.uk Password:2MzhUnon). The CUT&Tag data will be made available upon request and will be publicly available after publication.

## REFERENCES

1. Lavin Y, Mortha A, Rahman A, Merad M. Regulation of macrophage development and function in peripheral tissues. Nat Rev Immunol. 2015;15:731–44.
2. Murray PJ, Allen JE, Biswas SK, Fisher EA, Gilroy DW, Goerdt S, et al. Macrophage activation and polarization: nomenclature and experimental guidelines. Immunity. 2014;41:14–20.
3. Fleetwood AJ, Lawrence T, Hamilton JA, Cook AD. Granulocyte-macrophage colony-stimulating factor (CSF) and macrophage CSF-dependent macrophage phenotypes display differences in cytokine profiles and transcription factor activities: implications for CSF blockade in inflammation. J Immunol (Baltim, Md: 1950). 2007;178:5245–52.
4. Martinez FO, Gordon S. The M1 and M2 paradigm of macrophage activation: time for reassessment. F1000Prime Rep. 2014;6:13.
5. Verreck FA, de Boer T, Langenberg DM, Hoeve MA, Kramer M, Vaisberg E, et al. Human IL-23-producing type 1 macrophages promote but IL-10-producing type 2 macrophages subvert immunity to (myco)bacteria. Proc Natl Acad Sci USA. 2004;101:4560–5.
6. Hamilton JA. Colony-stimulating factors in inflammation and autoimmunity. Nat Rev Immunol. 2008;8:533–44.
7. Becher B, Tugues S, Greter M. GM-CSF: from growth factor to central mediator of tissue inflammation. Immunity. 2016;45:963–73.
8. Dranoff G, Jaffee E, Lazenby A, Golumbek P, Levitsky H, Brose K, et al. Vaccination with irradiated tumor cells engineered to secrete murine granulocyte-macrophage colony-stimulating factor stimulates potent, specific, and long-lasting anti-tumor immunity. Proc Natl Acad Sci USA. 1993;90:3539–43.
9. Bayne LJ, Beatty GL, Jhala N, Clark CE, Rhim AD, Stanger BZ, et al. Tumor-derived granulocyte-macrophage colony-stimulating factor regulates myeloid inflammation and T cell immunity in pancreatic cancer. Cancer cell. 2012;21:822–35.
10. Sielska M, Przanowski P, Wylot B, Gabrusiewicz K, Maleszewska M, Kijewska M, et al. Distinct roles of CSF family cytokines in macrophage infiltration and activation in glioma progression and injury response. J Pathol. 2013;230:310–21.
11. Bronte V, Chappell DB, Apolloni E, Cabrelle A, Wang M, Hwu P, et al. Unopposed production of granulocyte-macrophage colony-stimulating factor by tumors inhibits CD8+ T cell responses by dysregulating antigen-presenting cell maturation. J Immunol (Baltim, Md: 1950). 1999;162:5728–37.
12. Huen SC, Huynh L, Marlier A, Lee Y, Moeckel GW, Cantley LG. GM-CSF promotes macrophage alternative activation after renal ischemia/reperfusion injury. J Am Soc Nephrol. 2015;26:1334–45.
13. Cates EC, Fattouh R, Wattie J, Inman MD, Goncharova S, Coyle AJ, et al. Intranasal exposure of mice to house dust mite elicits allergic airway inflammation via a GM-CSF-mediated mechanism. J Immunol (Baltim, Md: 1950). 2004;173:6384–92.
14. Willart MA, Deswarte K, Pouliot P, Braun H, Beyaert R, Lambrecht BN, et al. Interleukin-1alpha controls allergic sensitization to inhaled house dust mite via the epithelial release of GM-CSF and IL-33. J Exp Med. 2012;209:1505–17.
15. Mills CD, Kincaid K, Alt JM, Heilman MJ, Hill AM. M-1/M-2 macrophages and the Th1/Th2 paradigm. J Immunol (Baltim, Md: 1950). 2000;164:6166–73.
16. Bernasconi E, Favre L, Maillard MH, Bachmann D, Pythoud C, Bouzourene H, et al. Granulocyte-macrophage colony-stimulating factor elicits bone marrow-derived cells that promote efficient colonic mucosal healing. Inflamm Bowel Dis. 2010;16:428–41.
17. Alexander WS, Hilton DJ. The role of suppressors of cytokine signaling (SOCS) proteins in regulation of the immune response. Annu Rev Immunol. 2004;22:503–29.
18. Louis C, Souza-Fonseca-Guimaraes F, Yang Y, D'silva D, Kratina T, Dagley L, et al. 2020. NK cell-derived GM-CSF potentiates inflammatory arthritis and is negatively regulated by CIS. J Exp Med. 217:e20191421
19. Feldman GM, Rosenthal LA, Liu X, Hayes MP, Wynshaw-Boris A, Leonard WJ, et al. STAT5A-deficient mice demonstrate a defect in granulocyte-macrophage colony-stimulating factor-induced proliferation and gene expression. Blood. 1997;90:1768–76.
20. Matsumoto A, Masuhara M, Mitsui K, Yokouchi M, Ohtsubo M, Misawa H, et al. CIS, a cytokine inducible SH2 protein, is a target of the JAK-STAT5 pathway and modulates STAT5 activation. Blood. 1997;89:3148–54.
21. Yoshimura A, Ohkubo T, Kiguchi T, Jenkins NA, Gilbert DJ, Copeland NG, et al. A novel cytokine-inducible gene CIS encodes an SH2-containing protein that binds to tyrosine-phosphorylated interleukin 3 and erythropoietin receptors. EMBO J. 1995;14:2816–26.
22. Lehtonen A, Matikainen S, Miettinen M, Julkunen I. Granulocyte-macrophage colony-stimulating factor (GM-CSF)-induced STAT5 activation and target-gene expression during human monocyte/macrophage differentiation. J Leukoc Biol. 2002;71:511–9.
23. Marine JC, McKay C, Wang D, Topham DJ, Parganas E, Nakajima H, et al. SOCS3 is essential in the regulation of fetal liver erythropoiesis. Cell. 1999;98:617–27.
24. Matsumoto A, Seki Y, Kubo M, Ohtsuka S, Suzuki A, Hayashi I, et al. Suppression of STAT5 functions in liver, mammary glands, and T cells in cytokine-inducible SH2-containing protein 1 transgenic mice. Mol Cell Biol. 1999;19:6396–407.
25. Delconte RB, Kolesnik TB, Dagley LF, Rautela J, Shi W, Putz EM, et al. CIS is a potent checkpoint in NK cell-mediated tumor immunity. Nat Immunol. 2016;17:816–24.
26. Palmer DC, Guittard GC, Franco Z, Crompton JG, Eil RL, Patel SJ, et al. Cish actively silences TCR signaling in CD8+ T cells to maintain tumor tolerance. J Exp Med. 2015;212:2095–113.
27. Yang XP, Ghoreschi K, Steward-Tharp SM, Rodriguez-Canales J, Zhu J, Grainger JR, et al. Opposing regulation of the locus encoding IL-17 through direct, reciprocal actions of STAT3 and STAT5. Nat Immunol. 2011;12:247–54.
28. Helft J, Bottcher J, Chakravarty P, Zelenay S, Huotari J, Schraml BU, et al. GM-CSF mouse bone marrow cultures comprise a heterogeneous population of CD11c(+) MHCII(+) macrophages and dendritic cells. Immunity. 2015;42:1197–211.
29. Henry CJ, Ornelles DA, Mitchell LM, Brzoza-Lewis KL, Hiltbold EM. IL-12 produced by dendritic cells augments CD8+ T cell activation through the production of the chemokines CCL1 and CCL17. J Immunol (Baltim, Md: 1950). 2008;181:8576–84.
30. Sun L, Rautela J, Delconte RB, Souza-Fonseca-Guimaraes F, Carrington EM, Schenk RL, et al. GM-CSF Quantity Has a Selective Effect on Granulocytic vs. Monocytic Myeloid Development and Function. Front Immunol. 2018;9:1922.
31. Chow KV, Lew AM, Sutherland RM, Zhan Y. Monocyte-derived dendritic cells promote th polarization, whereas conventional dendritic cells promote Th proliferation. J Immunol (Baltim, Md: 1950). 2016;196:624–36.
32. Erlich Z, Shlomovitz I, Edry-Botzer L, Cohen H, Frank D, Wang H, et al. Macrophages, rather than DCs, are responsible for inflammasome activity in the GM-CSF BMDC model. Nat Immunol. 2019;20:397–406.
33. Szanto A, Balint BL, Nagy ZS, Barta E, Dezso B, Pap A, et al. STAT6 transcription factor is a facilitator of the nuclear receptor PPARgamma-regulated gene expression in macrophages and dendritic cells. Immunity. 2010;33:699–712.
34. Pello OM, De Pizzol M, Mirolo M, Soucek L, Zammataro L, Amabile A, et al. Role of c-MYC in alternative activation of human macrophages and tumor-associated macrophage biology. Blood. 2012;119:411–21.
35. Martinez FO, Gordon S, Locati M, Mantovani A. Transcriptional profiling of the human monocyte-to-macrophage differentiation and polarization: new molecules and patterns of gene expression. J Immunol (Baltim, Md: 1950). 2006;177:7303–11.
36. Martinez FO, Helming L, Milde R, Varin A, Melgert BN, Draijer C, et al. Genetic programs expressed in resting and IL-4 alternatively activated mouse and human macrophages: similarities and differences. Blood. 2013;121:e57–69.
37. Lacey DC, Achuthan A, Fleetwood AJ, Dinh H, Roiniotis J, Scholz GM, et al. Defining GM-CSF- and macrophage-CSF-dependent macrophage responses by in vitro models. J Immunol (Baltim, Md: 1950). 2012;188:5752–65.
38. Rodriguez PC, Quiceno DG, Ochoa AC. L-arginine availability regulates T-lymphocyte cell-cycle progression. Blood. 2007;109:1568–73.
39. Bronte V, Serafini P, Mazzoni A, Segal DM, Zanovello P. L-arginine metabolism in myeloid cells controls T-lymphocyte functions. Trends Immunol. 2003;24:302–6.
40. Gunthner R, Anders HJ. Interferon-regulatory factors determine macrophage phenotype polarization. Mediators Inflamm. 2013;2013:731023.
41. Wang H, Yan M, Sun J, Jain S, Yoshimi R, Abolfath SM, et al. A reporter mouse reveals lineage-specific and heterogeneous expression of IRF8 during lymphoid and myeloid cell differentiation. J Immunol (Baltim, Md: 1950). 2014;193:1766–77.
42. Kurotaki D, Yamamoto M, Nishiyama A, Uno K, Ban T, Ichino M, et al. IRF8 inhibits C/EBPalpha activity to restrain mononuclear phagocyte progenitors from differentiating into neutrophils. Nat Commun. 2014;5:4978.
43. Kaya-Okur HS, Wu SJ, Codomo CA, Pledger ES, Bryson TD, Henikoff JG, et al. CUT&Tag for efficient epigenomic profiling of small samples and single cells. Nat Commun. 2019;10:1930.
44. Chávez-Galán L, Olleros ML, Vesin D, Garcia I. Much More than M1 and M2 Macrophages, There are also CD169(+) and TCR(+) Macrophages. Front Immunol. 2015;6:263.
45. Yang XO, Zhang H, Kim BS, Niu X, Peng J, Chen Y, et al. The signaling suppressor CIS controls proallergic T cell development and allergic airway inflammation. Nat Immunol. 2013;14:732–40.
46. Satoh T, Takeuchi O, Vandenbon A, Yasuda K, Tanaka Y, Kumagai Y, et al. The Jmjd3-Irf4 axis regulates M2 macrophage polarization and host responses against helminth infection. Nat Immunol. 2010;11:936–44.
47. Croxford AL, Lanzinger M, Hartmann FJ, Schreiner B, Mair F, Pelczar P, et al. The cytokine GM-CSF drives the inflammatory signature of CCR2+ monocytes and licenses autoimmunity. Immunity. 2015;43:502–14.

48. Ko HJ, Brady JL, Ryg-Cornejo V, Hansen DS, Vremec D, Shortman K, et al. GM-CSF-responsive monocyte-derived dendritic cells are pivotal in Th17 pathogenesis. J Immunol (Baltim, Md: 1950). 2014;192:2202–9.
49. Zhang Y, Li X, Luo Z, Ma L, Zhu S, Wang Z, et al. ECM1 is an essential factor for the determination of M1 macrophage polarization in IBD in response to LPS stimulation. Proc Natl Acad Sci USA. 2020;117:3083–92.
50. Bhattacharya P, Thiruppathi M, Elshabrawy HA, Alharshawi K, Kumar P, Prabhakar BS. GM-CSF: An immune modulatory cytokine that can suppress autoimmunity. Cytokine. 2015;75:261–71.
51. Esashi E, Wang YH, Perng O, Qin XF, Liu YJ, Watowich SS. The signal transducer STAT5 inhibits plasmacytoid dendritic cell development by suppressing transcription factor IRF8. Immunity. 2008;28:509–20.
52. Holtschke T, Lohler J, Kanno Y, Fehr T, Giese N, Rosenbauer F, et al. Immunodeficiency and chronic myelogenous leukemia-like syndrome in mice with a targeted mutation of the ICSBP gene. Cell. 1996;87:307–17.
53. Masumi A, Tamaoki S, Wang IM, Ozato K, Komuro K. IRF-8/ICSBP and IRF-1 cooperatively stimulate mouse IL-12 promoter activity in macrophages. FEBS Lett. 2002;531:348–53.
54. Ototake Y, Yamaguchi Y, Asami M, Komitsu N, Akita A, Watanabe T, et al. Downregulated IRF8 in Monocytes and Macrophages of Patients with Systemic Sclerosis May Aggravate the Fibrotic Phenotype. J investigative Dermatol. 2021;141:1954–63.
55. Twum DY, Colligan SH, Hoffend NC, Katsuta E, Gomez EC, Hensen ML, et al. IFN regulatory factor-8 expression in macrophages governs an antimetastatic program. JCI Insight. 2019;4:e124267
56. Waight JD, Netherby C, Hensen ML, Miller A, Hu Q, Liu S, et al. Myeloid-derived suppressor cell development is regulated by a STAT/IRF-8 axis. J Clin Investig. 2013;123:4464–78.
57. Cai Y, Kumar RK, Zhou J, Foster PS, Webb DC. Ym1/2 promotes Th2 cytokine expression by inhibiting 12/15(S)-lipoxygenase: identification of a novel pathway for regulating allergic inflammation. J Immunol (Baltim, Md: 1950). 2009;182:5393–9.
58. Arora M, Chen L, Paglia M, Gallagher I, Allen JE, Vyas YM, et al. Simvastatin promotes Th2-type responses through the induction of the chitinase family member Ym1 in dendritic cells. Proc Natl Acad Sci USA. 2006;103:7777–82.
59. Abdelaziz MH, Abdelwahab SF, Wan J, Cai W, Huixuan W, Jianjun C, et al. Alternatively activated macrophages; a double-edged sword in allergic asthma. J Transl Med. 2020;18:58.
60. Yates AD, Achuthan P, Akanni W, Allen J, Allen J, Alvarez-Jarreta J, et al. Ensembl 2020. Nucleic Acids Res. 2020;48:D682–D688.
61. Bray NL, Pimentel H, Melsted P, Pachter L. Near-optimal probabilistic RNA-seq quantification. Nat Biotechnol. 2016;34:525–7.
62. Roguev A, Talbot D, Negri GL, Shales M, Cagney G, Bandyopadhyay S, et al. Quantitative genetic-interaction mapping in mammalian cells. Nat Methods. 2013;10:432–7.
63. Yi L, Pimentel H, Bray NL, Pachter L. Gene-level differential analysis at transcript-level resolution. Genome Biol. 2018;19:53.
64. Benjamini Y, Hochberg Y. Controlling the false discovery rate: a practical and powerful approach to multiple testing. J R Stat Soc: Ser B (Methodol). 1995;57:289–300.
65. Wagner GP, Kin K, Lynch VJ. Measurement of mRNA abundance using RNA-seq data: RPKM measure is inconsistent among samples. Theory Biosci. 2012;131:281–5.
66. Ritchie ME, Phipson B, Wu D, Hu Y, Law CW, Shi W, et al. limma powers differential expression analyses for RNA-sequencing and microarray studies. Nucleic Acids Res. 2015;43:e47.
67. Rautela J, Dagley LF, De Oliveira CC, Schuster IS, Hediyeh-Zadeh S, Delconte RB, et al. Therapeutic blockade of activin-A improves NK cell function and antitumor immunity. Sci Signal. 2019;12:eaat7527
68. Mezger A, Klemm S, Mann I, Brower K, Mir A, Bostick M, et al. High-throughput chromatin accessibility profiling at single-cell resolution. Nat Commun. 2018;9:3647.
69. Langmead B, Salzberg SL. Fast gapped-read alignment with Bowtie 2. Nat Methods. 2012;9:357–9.
70. Langmead B, Trapnell C, Pop M, Salzberg SL. Ultrafast and memory-efficient alignment of short DNA sequences to the human genome. Genome Biol. 2009;10:R25.
71. Feng J, Liu T, Qin B, Zhang Y, Liu XS. Identifying ChIP-seq enrichment using MACS. Nat Protoc. 2012;7:1728–40.
72. Zhang Y, Liu T, Meyer CA, Eeckhoute J, Johnson DS, Bernstein BE, et al. Model-based analysis of ChIP-Seq (MACS). Genome Biol. 2008;9:R137.
73. Nicol JW, Helt GA, Blanchard SG Jr., Raja A, Loraine AE. The Integrated Genome Browser: free software for distribution and exploration of genome-scale datasets. Bioinforma (Oxf, Engl). 2009;25:2730–1.
74. Yu G, Wang LG, He QY. ChIPseeker: an R/Bioconductor package for ChIP peak annotation, comparison and visualization. Bioinforma (Oxf, Engl). 2015;31:2382–3.
75. Quinlan AR, Hall IM. BEDTools: a flexible suite of utilities for comparing genomic features. Bioinforma (Oxf, Engl). 2010;26:841–2.
76. Keenan CR, Iannarella N, Garnham AL, Brown AC, Kim RY, Horvat JC, et al. Polycomb repressive complex 2 is a critical mediator of allergic inflammation. JCI Insight. 2019;4:e127745.

## ACKNOWLEDGEMENTS

We thank Lisa Reid, Marina Patsis, Manuela Hancock, Rhiannan Crawley, Rebekah Meeny, Tania Camilleri, and the institute flow cytometry facility for excellent technical assistance. We acknowledge the Wurundjeri people of the Kulin nation as the traditional owners and guardians of the land on which most of the work was performed. This work was supported by National Health and Medical Research Council of Australia (NHMRC) grants (1037321, 1105209, 1143976, 1150425, 1080321, 1196335, 5575500, 1054925, and 1048278), an NHMRC Independent Research Institutes Infrastructure Support Scheme grant (361646) and a Victorian State Government Operational Infrastructure Support grant. JB was supported by the Stafford Fox Medical Research Foundation.

## AUTHOR CONTRIBUTIONS

Conceptualization, YZ; Methodology: SBZ, JR, MC, NGB, LFD, JB, YY, and YX; Investigation: YZ, SBZ, TBK, JR, MC, QKW, HQW, LS, RS, LFD, FSFG, YY, YX, RA, NI, and JLN; Writing—Original Draft, YZ with input from SBZ, AML, SN, SEN, MC, NGB, and YY; Review & Editing: SBZ, MC, NGB, LFD, YKX, SN, NDH, SEN, and AML; and Resources: JR, NDH, SN, and SEN.

## COMPETING INTERESTS

The authors declare no competing interests.

## ADDITIONAL INFORMATION

**Supplementary information** The online version contains supplementary material available at https://doi.org/10.1038/s41423-022-00957-z.

**Correspondence** and requests for materials should be addressed to Michaël Chopin or Yifan Zhan.

**Reprints and permission information** is available at http://www.nature.com/reprints